Progress in Oceanography 88 (2011) 59–77

Contents lists available at ScienceDirect

Progress in Oceanography

journal homepage: www.elsevier.com/locate/pocean

Seasonal and inter-annual variability of air–sea CO_2 fluxes and seawater carbonate chemistry in the Southern North Sea

N. Gypens [a,*], G. Lacroix [b], C. Lancelot [a], A.V. Borges [c]

[a] Université Libre de Bruxelles, Faculté des Sciences, Ecologie des Systèmes Aquatiques, CP-221, Bd du Triomphe, B-1050, Belgium
[b] Management Unit of the North Sea Mathematical Models, Royal Belgian Institute of Natural Sciences, 100 Gulledelle, B-1200 Brussels, Belgium
[c] Université de Liège, Unité d'Océanographie Chimique, Institut de Physique (B5), B-4000, Belgium

ARTICLE INFO

Article history:
Received 9 February 2010
Received in revised form 23 November 2010
Accepted 23 November 2010
Available online 2 December 2010

ABSTRACT

A 3D coupled biogeochemical–hydrodynamic model (MIRO-CO_2&CO) is implemented in the English Channel (ECH) and the Southern Bight of the North Sea (SBNS) to estimate the present-day spatio-temporal distribution of air–sea CO_2 fluxes, surface water partial pressure of CO_2 (pCO_2) and other components of the carbonate system (pH, saturation state of calcite (Ω_{ca}) and of aragonite (Ω_{ar})), and the main drivers of their variability. Over the 1994–2004 period, air–sea CO_2 fluxes show significant inter-annual variability, with oscillations between net annual CO_2 sinks and sources. The inter-annual variability of air–sea CO_2 fluxes simulated in the SBNS is controlled primarily by river loads and changes of biological activities (net autotrophy in spring and early summer, and net heterotrophy in winter and autumn), while in areas less influenced by river inputs such as the ECH, the inter-annual variations of air–sea CO_2 fluxes are mainly due to changes in sea surface temperature and in near-surface wind strength and direction. In the ECH, the decrease of pH, of Ω_{ca} and of Ω_{ar} follows the one expected from the increase of atmospheric CO_2 (ocean acidification), but the decrease of these quantities in the SBNS during the considered time period is faster than the one expected from ocean acidification alone. This seems to be related to a general pattern of decreasing nutrient river loads and net ecosystem production (NEP) in the SBNS. Annually, the combined effect of carbon and nutrient loads leads to an increase of the sink of CO_2 in the ECH and the SBNS, but the impact of the river loads varies spatially and is stronger in river plumes and nearshore waters than in offshore waters. The impact of organic and inorganic carbon (C) inputs is mainly confined to the coast and generates a source of CO_2 to the atmosphere and low pH, of Ω_{ca} and of Ω_{ar} values in estuarine plumes, while the impact of nutrient loads, highest than the effect of C inputs in coastal nearshore waters, also propagates offshore and, by stimulating primary production, drives a sink of atmospheric CO_2 and higher values of pH, of Ω_{ca} and of Ω_{ar}.

1. Introduction

Global estimates of air–sea CO_2 fluxes suggest that the coastal ocean is a significant sink for atmospheric CO_2 with values converging to 0.2 Pg C yr^{-1} (Borges, 2005; Borges et al., 2005; Cai et al., 2006; Chen and Borges, 2009; Laruelle et al., 2010). This adds some 20% to the contemporary open ocean CO_2 sink based on the most recent climatology of the surface partial pressure of CO_2 (pCO_2) (Takahashi et al., 2009). Besides changes in the capacity of coastal waters to absorb atmospheric CO_2, human activities on the watersheds and the increase of atmospheric CO_2 have altered the other components of the carbonate chemistry in surface waters (Borges and Gypens, 2010). Ocean acidification is related to the input of anthropogenic CO_2 to surface oceans from the atmosphere, leading to shifts in carbonate chemistry (increase of CO_2, decrease of pH, of CO_3^{2-}, of the saturation state of calcite (Ω_{ca}) and of aragonite (Ω_{ar})) that can lead to changes in the rates and fates of primary production and calcification of marine organisms and communities (e.g., reviews by Kleypas et al. (2006), Fabry et al. (2008) and Doney et al. (2009)). In coastal environments, besides ocean acidification, seawater carbonate chemistry can be affected (among others) by biological activity (e.g. Borges and Gypens, 2010), by anthropogenic atmospheric nitrogen and sulfur deposition (Doney et al., 2007), by upwelling of anthropogenically "acidified" dissolved inorganic carbon (DIC)-rich waters (Feely et al., 2008), or by river inputs (Gledhill et al., 2008; Salisbury et al., 2008, 2009; Chierici and Fransson, 2009).

Freshwater inputs of nutrient and organic matter in coastal ecosystems have an opposite impact on carbonate chemistry by, respectively, stimulating autotrophy (primary production) and heterotrophy (microbial degradation of organic matter). Consequently,

* Corresponding author. Tel.: +32 26505924; fax: +32 26505993.
E-mail address: ngypens@ulb.ac.be (N. Gypens).

0079-6611/$ - see front matter © 2010 Elsevier Ltd. All rights reserved.
doi:10.1016/j.pocean.2010.11.004

coastal ecosystems influenced by continental loads can act either as a net source of CO_2 to the atmosphere (Cai and Wang, 1998; Borges and Frankignoulle, 1999, 2002; Algesten et al., 2004) or as a significant sink for atmospheric CO_2 (Tsunogai et al., 1999; Liu et al., 2000; Körtzinger, 2003; Thomas et al., 2004) and the direction of air–sea CO_2 fluxes can vary over time (Gypens et al., 2009; Omstedt et al., 2009; Wesslander et al., 2010). Additionally, coastal ecosystems are characterized by very strong horizontal gradients and temporal changes explaining why opposite annual air–sea CO_2 flux estimates in a given coastal environment have been reported due to either sparse temporal coverage (e.g. the Southern Bight of the North Sea (SBNS); compare Thomas et al. (2004) and Schiettecatte et al. (2007)) or inadequate geographical grid sampling (e.g. US South Atlantic Bight; compare Cai et al. (2003) and Jiang et al. (2008)). Consequently, highly-resolved spatial and temporal coverage of pCO_2 is required to assess the annual air–sea CO_2 and the effects of anthropogenic pressures and their modifications, and ocean acidification in coastal ecosystems. Mathematical models with ad hoc spatio-temporal resolution can be used to make up for the sparse coverage of pCO_2 field data and provide robust air–sea CO_2 flux estimates and a more rigorous analysis of the biotic and abiotic processes controlling the dynamics of seawater carbonate system.

Due to its shallow depths and strong tidal currents, the SBNS (from the Dover Strait to 53°N) is a highly dynamic and permanently well-mixed coastal area that receives high inputs of nutrients and organic and inorganic carbon from the Scheldt, Rhine/Meuse and Thames rivers, and indirectly from the Seine and Somme through inputs from the English Channel (ECH) across the Dover Strait (Fig. 1). Existing measurements of pCO_2 show that the SBNS is characterized by a strong spatial and seasonal variability (from 100 to 800 ppm) under the control of river loads and the related biological (autotrophic and heterotrophic) activity (Kempe and Pegler, 1991; Hoppema, 1991; Bakker et al., 1996; Frankignoulle and Borges, 2001; Borges and Frankignoulle, 1999, 2002, 2003; Thomas et al., 2004; Schiettecatte et al., 2006, 2007; Borges et al., 2008a; Omar et al., 2010). These studies report a broad range of pCO_2 and air–sea CO_2 flux values resulting from the lack of adequate temporal and/or spatial coverage but also because these studies were carried out during the eighties and the nineties, i.e. a period of intensive changes in land use and human activities in the watershed (Billen et al., 2001, 2005) that greatly affected carbon and nutrient inputs to coastal waters (Lancelot et al., 2007), the direction of the air–sea CO_2 fluxes (Gypens et al., 2009) and consequently the seawater carbonate chemistry (Borges and Gypens, 2010).

In a first attempt of using modelling tools to unravel the CO_2 dynamics in the *Phaeocystis*-dominated SBNS ecosystem, the MIRO-CO_2 model was implemented in a 0D multi-box configuration in the Eastern English Channel and the Belgian coastal zone (BCZ) for the description of present-day seasonality (Gypens et al., 2004) and for the historical reconstruction over the 1951–1998 period (Gypens et al., 2009; Borges and Gypens, 2010). Model results revealed that riverine nutrient and carbon loads largely controlled the magnitude and direction of the air–sea CO_2 fluxes in the BCZ, and that at decadal time scales, due to changes in nutrient river loads, the BCZ shifted from a CO_2 source to a CO_2 sink from the 1950s to mid-1980s and back to a CO_2 source in the late 1990s. These studies focussed on the BCZ, and did not allow describing the CO_2 dynamics and air–sea CO_2 fluxes in the whole of the SBNS that is influenced by major European rivers such as the Rhine and the Thames.

In this paper, to understand the spatio-temporal variability of air–sea CO_2 fluxes and other seawater carbonate chemistry variables (pH, Ω_{ca} and Ω_{ar}), we use the 3D coupled biogeochemical–hydrodynamical model MIRO-CO_2&CO implemented in the ECH and the SBNS from 1994 to 2004. Several sensitivity tests are performed to determine the role of biological activity, changes in sea surface temperature (SST) and river inputs (nutrients, organic and inorganic carbon) on the simulated spatial and seasonal variability of air–sea CO_2 fluxes and seawater carbonate chemistry variables. Furthermore, inter-annual variability of air–sea CO_2 fluxes and seawater carbonate chemistry variables are investigated for the 1994–2004 period and the impact of the different forcing (SST, wind speed strength and direction, atmospheric pCO_2 increase and river loads variability) estimated.

2. Model description

The mathematical tool (MIRO-CO_2&CO) couples the chemical module describing the seawater carbonate chemistry and air–sea

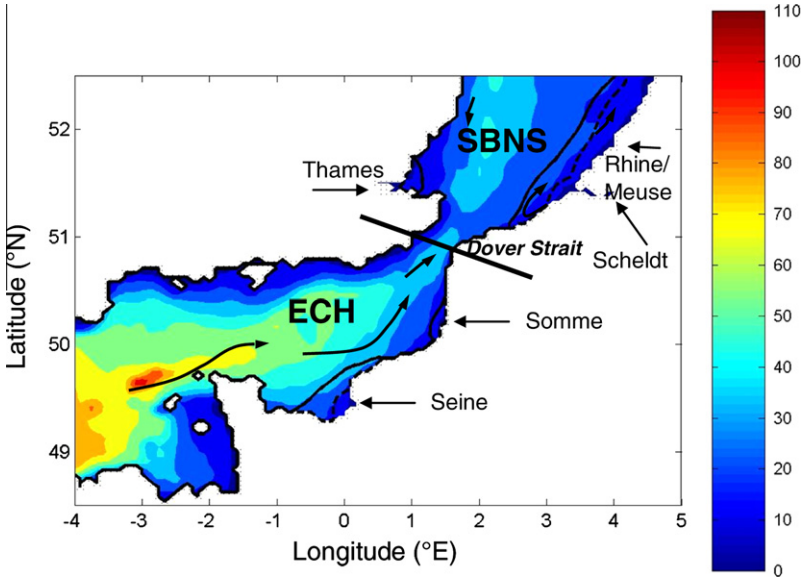

Fig. 1. Bathymetry (in m) of the English Channel and the Southern Bight of the North Sea with schematic advection (black arrows) and the different regions defined based on sea surface salinity (SSS) (nearshore SSS < 32 (dotted line), intermediate 32 < SSS < 34 (solid line), and offshore SSS > 34) simulated by the model for the 1994–2004 period. The black line at the Dover Strait separates the English Channel and the Southern Bight of the North Sea as defined in this study.

CO_2 exchange (Gypens et al., 2004, 2009) to the biogeochemical MIRO&CO-3D model (Lacroix et al., 2007a,b).

2.1. MIRO&CO-3D model

MIRO&CO-3D results of the coupling between the 3D hydrodynamical model COHSNS (Lacroix et al., 2004) and the biogeochemical MIRO model (Lancelot et al., 2005) and simulates the transport and dynamics of inorganic and organic nutrients, phytoplankton, bacterioplankton and zooplankton in the ECH and the SBNS. The biogeochemical MIRO model, describing C, N, P and Si cycles in *Phaeocystis*-dominated ecosystems, assembles four main modules describing the dynamics of phytoplankton (diatoms, nanoflagellates and *Phaeocystis*), zooplankton (copepods and microzooplankton), the degradation of dissolved and particulate organic matter (each with two classes of biodegradability) and the regeneration of inorganic nutrients (NO_3^-, NH_4^+, PO_4^{3-} and $Si(OH)_4$) by bacteria in the water column and the sediment. Equations and parameters were formulated based on current knowledge of the kinetics and the factors controlling the main auto- and heterotrophic processes involved in the functioning of the coastal marine ecosystem (fully documented by Lancelot et al. (2005) and in http://www.int-res.com/journals/suppl/appendix_lancelot.pdf).

2.2. The seawater carbonate chemistry module

The seawater carbonate chemistry module adds two state variables, DIC and total alkalinity (TA), for the description of the carbonate system in seawater and the evaluation of the exchange of CO_2 across the air–sea interface. The speciation of the carbonate system (pCO_2 and pH) is calculated from DIC and TA, using the carbonic acid dissociation constants given by Mehrbach et al. (1973), the boric acid dissociation constant given by Dickson (1990), and the CO_2 solubility coefficient given by Weiss (1974). The saturation state of Ω_{ca} and Ω_{ar} are computed from simulated surface pCO_2, TA, sea surface salinity (SSS) and SST, using the calcite and aragonite solubility given by Mucci (1983). Air–sea CO_2 fluxes are calculated from the pCO_2 gradient across the air–sea interface ($\Delta pCO_2 = pCO_2 - pCO_{2atm}$, where pCO_{2atm} refers to values in the atmosphere) and the gas transfer velocity parameterization as a function of wind speed of Nightingale et al. (2000).

2.3. MIRO-CO_2&CO model implementation and data

MIRO-CO_2&CO was implemented in the region between 48.5°N and 52.5°N, and between 4°W and 5°E (Fig. 1), using a 109×97 horizontal grid with a resolution of 5′ longitude (~5.6 km) by 2.5′ latitude (~4.6 km) and with five vertical sigma coordinate layers. The ECH and SBNS domains defined in this study are comprised between 3°W and 2°E and between 2°E and 5°E, respectively, and connected by the Strait of Dover (Fig. 1). Model simulations were conducted from 1991 to 2004, using initial and open boundary conditions given by Lacroix et al. (2007b). To reduce the sensitivity of model results to initial conditions, a spin-up was run for the period January 1991–December 1993. The reference simulation was then run from January 1994 to December 2004.

The coupled model is forced by 6-hourly wind and atmospheric pressure fields from the re-analyzed forecast data of the UK Meteorological Office. The wind forcing is spatially variable on a grid with resolution ranging from 1.25° to 5.00° in longitude and 1.25° to 2.50° in latitude (Lacroix et al., 2004). Temperature fields are obtained by computing advection/diffusion of observed SST imposed at the surface (instead of being computed from heat fluxes). SST weekly gridded fields (20 km × 20 km) were obtained from Bundesamt fuer Seeschiffahrt und Hydrographie (BSH, http://www.bsh.de/) (Loewe, 2003). They have been adapted to the model grid and temporally interpolated over the model time step. For periods without SST data (1991–1995), a weekly climatological SST field (computed from 1996–2000 BSH data) has been used. Monthly atmospheric pCO_2 values from Mace Head (53.55°N 9.00°W, southern Ireland) are imposed in the whole domain and were obtained from the National Oceanic and Atmospheric Administration/Climate Monitoring and Diagnostics Laboratory/Carbon Cycle Greenhouse Gases Group air sampling network (available at http://www.cmdl.noaa.gov/).

River discharges, inputs of inorganic (NO_3^-, NH_4^+, PO_4^{3-}, $Si(OH)_4$) and organic (Norg, Porg) nutrient and organic carbon were retrieved from existing databases (Tables 1 and 2 in Lacroix et al., 2007b; Fig. 2b–d). River inputs of DIC and TA were estimated based on a compilation of data available for the Thames, Rhine, Seine and Scheldt rivers (Frankignoulle et al., 1996, 1998; Borges, Unpublished data; Abril, personal communication; Biogas transfer in estuaries (BIOGEST) data-base http://www.co2.ulg.ac.be/biogest/). For the several small rivers (corresponding to 3% of the total annual freshwater discharge) for which no DIC and TA data are available, we used the averaged concentrations estimated for the Thames, Rhine, Seine and Scheldt rivers.

2.4. Models validation

The MIRO&CO-3D model was previously validated using: (i) 1991–2003 time series of salinity (Lacroix et al., 2004), NO_3^-, NH_4^+, PO_4^{3-}, $Si(OH)_4$, chlorophyll a (Chl *a*), diatom and *Phaeocystis* biomass (Lacroix et al., 2007b) at station 330 (51.43°N; 2.8°E) of the Belgian monitoring programme, (ii) 1993–2003 seasonal surface averaged concentrations of inorganic nutrients and Chl *a* at several stations from different national monitoring programs (BE, FR, NL, UK) (Lacroix et al., 2007a) and (iii) remote sensed Chl *a* (Lacroix et al., 2007b).

These comparisons have shown the ability of the model to represent the seasonal dynamics of nutrients and phytoplankton in the SBNS. The spatial distribution of surface winter nutrients is generally well reproduced by the model with a small overestimation for a few stations close to the Rhine mouth and a tendency for underestimation in the coastal zone from Belgium to France. Phosphate concentration was simulated best; silica concentration was simulated with less success. The accuracy of the simulated phytoplankton spatial distribution, evaluated by comparing simulated surface Chl *a* with that derived from the satellite sensor MERIS for the year 2003, showed a reasonable agreement with nevertheless an underestimation of Chl *a* in spring and discrepancies close to the boundaries (Lacroix et al., 2007b).

A first validation of the carbonate module in the region of interest was performed by comparing pCO_2, DIC and TA simulations obtained with the 0D multi-box version of the model (MIRO-CO_2) for the 1996–1999 period in the BCZ with available field data (Gypens et al., 2004). The simulated pCO_2 and DIC and TA concentrations were successfully compared with data recorded over the same period in the central BCZ at station 330 (51°26.050′N; 2°48.500′E) with a small underestimation of the late summer-early autumn CO_2 over-saturation. The simulated DIC and pCO_2 reached lowest values at the time of phytoplankton bloom peak and increased in mid-May when heterotrophs prevailed over autotrophs. The highest TA values were modelled in late April–early May when phytoplankton biomass was elevated and consumed NO_3^-. Lowest TA were simulated in late fall when phytoplankton growth had ceased but heterotrophic process and nitrification were still operating (Gypens et al., 2004).

In this paper, MIRO-CO_2&CO model results for pCO_2 will be weekly averaged and compared with available pCO_2 data sets for years 2003 and 2004 (Schiettecatte et al., 2007), available from

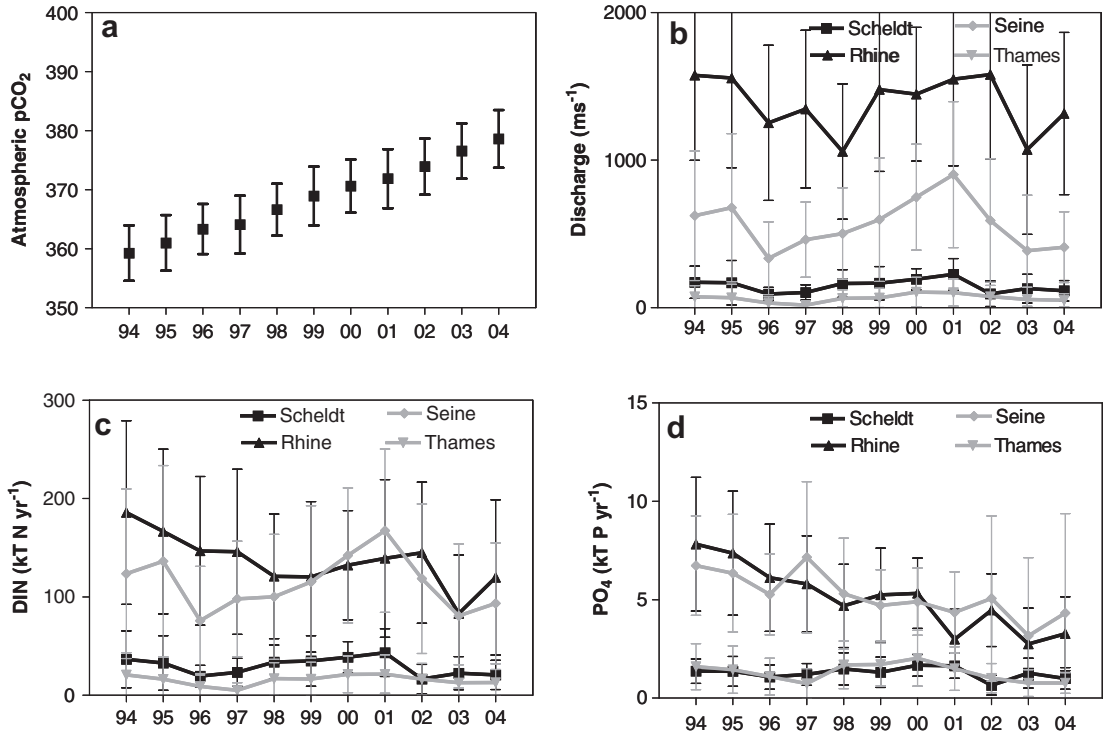

Fig. 2. Mean annual: (a) atmospheric pCO_2 (ppm) applied to whole model domain, (b) freshwater discharge, (c) dissolved inorganic nitrogen loads (kT N yr^{-1}) and (d) PO_4 loads (kT P yr^{-1}) from the Scheldt, Rhine, Thames and Seine rivers between 1994 and 2004. Error bars correspond to the standard deviation on the annual mean.

the Belgian marine data centre (http://www.mumm.ac.be/data-centre/).

2.5. EOF analysis

Empirical Orthogonal Function (EOF) is used to estimate spatial and temporal (seasonal and inter-annual) patterns of variability. The EOF analysis is a standard technique used to identify the main modes of variability of a time series. Since the EOF analysis depends on the decomposition of a covariance matrix, the traditional approach is based on the method of moments (MOM) estimation procedure (e.g. Wikle, 2002), implying that some mean term is estimated and removed in order to compute the covariance. In our case, EOFs are calculated using singular value decomposition and a temporal average is removed from the simulations. EOFs will be computed using a monthly and an annual time step to estimate respectively the seasonal and inter-annual variability.

3. Results and discussion

3.1. MIRO-CO_2&CO validation

Fig. 3 compares weekly averaged modelled and measured surface pCO_2 during different periods in 2003–2004, covering the seasonal cycle. Both observations and model results point large spatial and seasonal variations of surface pCO_2 in the whole domain, with the highest under- and over-saturations of CO_2 (i.e. seasonal amplitude of pCO_2) with respect to atmospheric equilibrium (~377 ppm in 2004) in the vicinity of the river mouths. As a general pattern, the simulated spatio-temporal variability of surface pCO_2 is lower in the offshore waters of the ECH than in the SBNS with values ranging between ~100 and ~700 ppm (Fig. 3).

In winter, measured and simulated pCO_2 (from ~350 to ~370 ppm) are lower but close to atmospheric equilibrium in the whole domain except in the vicinity of the river mouths characterized by CO_2 over-saturation (~500 to ~670 ppm) (Fig. 3c). In spring (Fig. 3d and e), the spatial gradients and the temporal variability of surface pCO_2 are more intense than during the other seasons (Fig. 3a, b, c and f). High horizontal gradients are simulated in early spring (Fig. 3d) when offshore waters are still close to the atmospheric CO_2 equilibrium, coastal waters are significantly CO_2 undersaturated (pCO_2 down to 100 ppm; Fig. 3d) and CO_2 over-saturation prevails nearshore in the vicinity of rivers discharging in the SBNS (Scheldt, Rhine and Thames), in agreement with observations (Fig. 3d). Four weeks later (Fig. 3e), a significant CO_2 undersaturation is simulated in the whole domain, due to spring primary production (not shown), except in the turbid Thames plume where CO_2 over-saturation prevails in the model and is higher than in the field measurements. During summer (Fig. 3a), observed pCO_2 patterns suggest over-saturation in the whole domain, especially nearshore. Simulated pCO_2 fields show similar patterns except nearshore where the model fails to reproduce the marked CO_2 over-saturation measured in the Scheldt river plume (Fig. 3a). In autumn, CO_2 over-saturation is simulated in the whole domain, with the highest CO_2 over-saturation near the river mouths (mainly in the Rhine and Scheldt plumes) in agreement with observations (Fig. 3b,f).

Altogether the model describes satisfactorily the main patterns (timing, magnitude, amplitude, horizontal gradients) of the observed spatial and temporal variability of surface pCO_2 in the SBNS in 2003 and 2004. The largest differences between observations and simulations are found in the nearshore waters of the Seine and the Scheldt estuaries in summer and in the vicinity of the Thames in late spring. Discrepancies between field measurements and model results could partly result from the SST and/or the suspended particulate matter (SPM) forcing used in the model. These two quantities show important spatial and temporal variability that might not be captured by the model that uses a weekly and a seasonal resolution for SST and SPM, respectively.

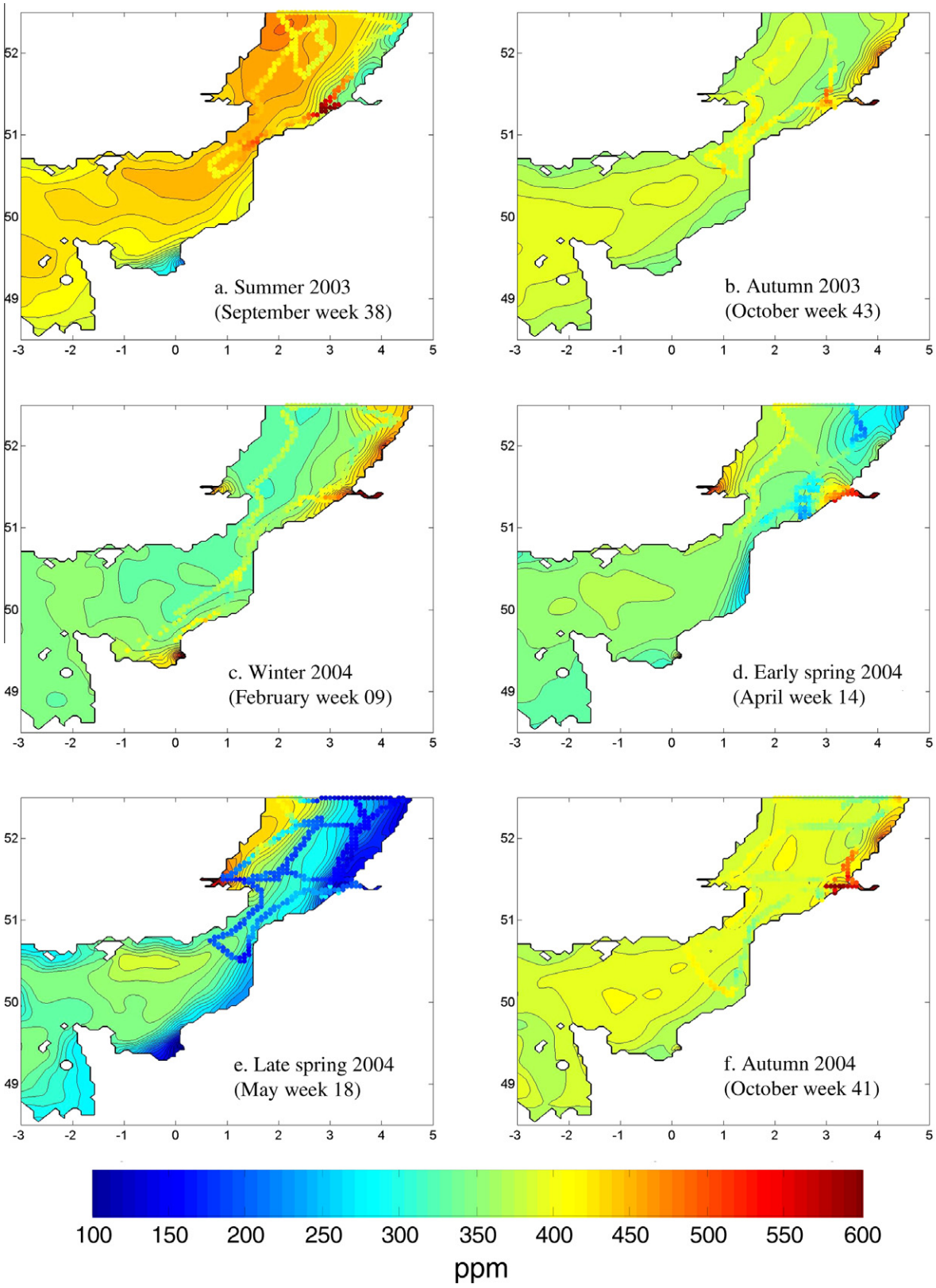

Fig. 3. Spatial distribution of surface pCO_2 (ppm) measured (dotted points) and simulated for different weeks of years 2003 and 2004 in the English Channel and Southern Bight of the North Sea.

Fig. 4 compares mean weekly modelled and measured surface pCO_2 (Fig. 4a) and pCO_2 normalized to a temperature of 13 °C (pCO_2@13 °C, Fig. 4b) for the different measurement periods of the years 2003–2004 (nine sampling periods including those presented in Fig. 3). Simulated results were extracted at the exact location of the field measurements and averaged for each period

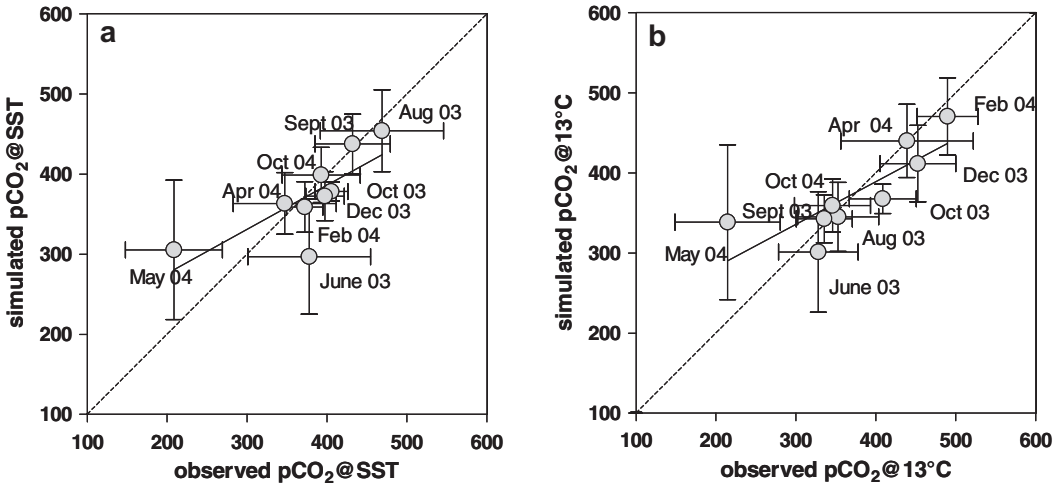

Fig. 4. Comparison of the mean weekly modelled and measured surface pCO_2 and pCO_2 (ppm) normalized to a temperature of 13 °C (pCO_2@13 °C) for the different measurement periods of the years 2003–2004, the error bars correspond to the spatial variability observed or modelled during the considered period of time. Simulated results were extracted at the exact location of the field measurement and averaged for each period. Dotted line corresponds to 1:1 line, solid line corresponds to linear regression.

(Fig. 4). The largest model/field differences are observed in spring/early summer (Fig. 4a), when simulations underestimate and overestimate pCO_2 compared to observations in June 2003 and May 2004, respectively (Fig. 4a). The comparison of pCO_2@13 °C (Fig. 4b) shows that the modelled and observed values are in better agreement in June 2003 and that the discrepancy of pCO_2 computed during this period is due to differences between SST given by the model and *in situ* measurements. However, the comparison of pCO_2@13 °C still shows a discrepancy between modelled and observed values in May 2004. In particular, model results and measured data differ along the British coast, while surface water CO_2 under-saturation is correctly reproduced by the model along the Belgian and the Dutch coasts and in the central SBNS (Fig. 3). The Thames river plume is characterized by higher SPM values than the other river plumes in the SBNS (e.g. Mills et al., 1994; Lacroix et al., submitted for publication). Although the low field data coverage in this area does not allow to unambiguously validate the model simulations, the strong CO_2 over-saturation simulated in spring could be due to the fields of SPM used to force the model.

The discrepancies observed in summer 2003 (Fig. 3a) in the nearshore Belgian and Dutch waters disappear when considering the averaged value of whole sampling points (Fig. 4a). Considering that these discrepancies only concern the most nearshore coastal grid points of the model, they will only marginally affect the analysis of the drivers of seasonal and inter-annual variations given hereafter at the scale of the SBNS.

3.2. Seasonal and spatial variability of the carbonate system variables

3.2.1. Surface pCO_2 and pH

As observed in 2003–2004 (Fig. 3), modelled surface pCO_2 averaged for the 1994–2004 period (Fig. 5) is characterized by an important seasonal cycle, with surface waters successively oversaturated (summer and autumn) and undersaturated (spring) compared to atmospheric CO_2 equilibrium and characterized by important horizontal gradients with the highest amplitude of variation simulated in the nearshore coastal waters (with values between <100 and 700 ppm).

The spatio-temporal variations of pH follow closely those of surface pCO_2 in the whole domain (Fig. 5). Modelled winter pH ranges between 7.95 and 8.07 in offshore waters. Nearshore waters, especially river plumes, show pH values down to 7.95 due to the CO_2 release from organic matter degradation. A significant increase of pH is simulated in spring and summer in nearshore waters (values up to 8.60; Fig. 5b and c) due to the CO_2 net uptake by phytoplankton in spring and to a lesser extent in summer. During autumn (Fig. 5d), pH values in nearshore waters are lower (values down to 7.95 near the Scheldt and the Thames) than in offshore waters (values up to 8.07) due to the dominance of heterotrophic processes releasing CO_2 (Fig. 10).

3.2.2. Ω_{ca} and Ω_{ar}

The spatial and seasonal variability of Ω_{ca} and Ω_{ar} is closely related to changes in biological activity. However, the seasonal variability of Ω_{ca} and Ω_{ar} in the domain is also controlled by temperature, with average values higher during summer (3.38 and 2.21 for Ω_{ca} and Ω_{ar}, respectively; Fig. 6c) than during winter (2.62 and 1.68 for Ω_{ca} and Ω_{ar}, respectively; Fig. 6a). For constant TA and DIC conditions, Ω_{ca} and Ω_{ar} increase by ~0.02 for each °C of temperature increase, as calculated with the constants of Mucci (1983); giving for Ω an increase of around 0.2 between winter and summer. During autumn (Fig. 6d) and winter (Fig. 6a), Ω_{ca} and Ω_{ar} values are lower in the nearshore waters associated with river plumes than in offshore waters, in relation to higher CO_2 and lower pH values (hence lower CO_3^{2-}) due to the degradation of organic matter that dominates primary production (Fig. 10). Conversely, during spring (Fig. 6b) and summer (Fig. 6c), Ω_{ca} and Ω_{ar} values are higher in the nearshore waters associated with river plumes than in offshore waters, in relation to lower CO_2 and higher pH values (hence higher CO_3^{2-}) due to autotrophy dominance. In contrast to what we report in the SBNS, river plumes in other parts of the world can be characterized by very low Ω_{ca} and Ω_{ar} (even <1, i.e. $CaCO_3$ under-saturation) such as the Kennebec river plume (Salisbury et al., 2008) and over the Mackenzie shelf (Chierici and Fransson, 2009). This different behaviour in Ω_{ca} and Ω_{ar} in river plumes is related to much lower TA freshwater end-members (Kennebec river ~300 μmol kg^{-1}, Salisbury, personal communication; Mackenzie river ~1800 μmol kg^{-1} (Cai et al., 2008)) compared to those of rivers bordering the SBNS (ranging between ~2700 and ~4000 μmol kg^{-1} for the Rhine and both the Thames and Scheldt, respectively).

3.2.3. Air–sea CO_2 fluxes

Fig. 7 shows the monthly climatology of air–sea CO_2 fluxes integrated over the whole simulated domain and estimated for the 1994–2004 period. Surface waters act as a sink for atmospheric

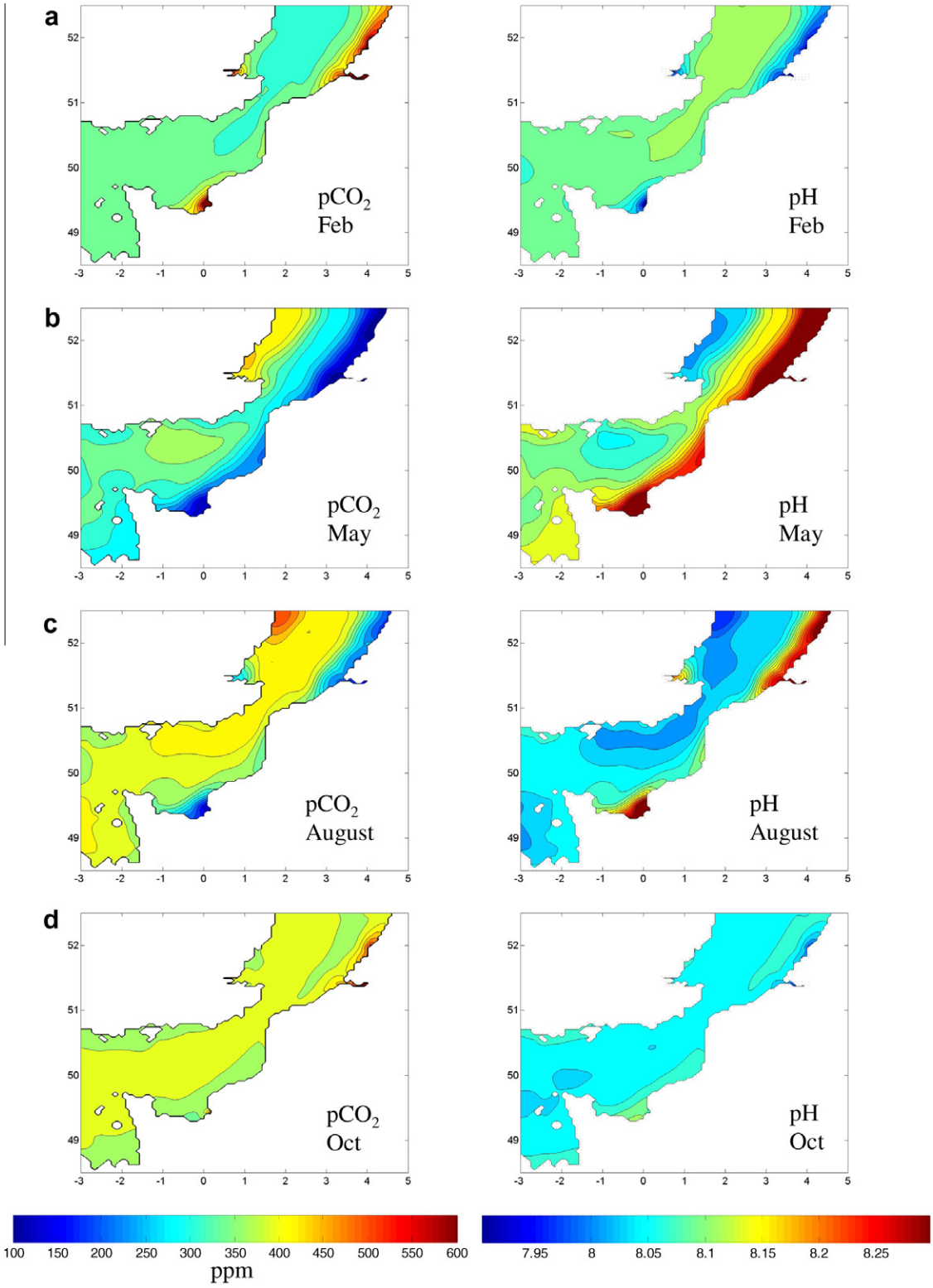

Fig. 5. Spatial distribution of climatological (1994–2004) monthly averaged surface pCO_2 (left panels) and pH (right panels) simulated in February, May, August and October, in the English Channel and Southern Bight of the North Sea.

CO_2 from December to June (-0.6 ± 4.6 to -3.5 ± 4.6 mmol C m^{-2} d^{-1}) and as a source of atmospheric CO_2 (0.3 ± 3.3 to 3.7 ± 2.3 mmol C m^{-2} d^{-1}) from July to November, in fair agreement with the seasonality of air–sea CO_2 fluxes based on a compilation of data from different years (1993–1999) reported by Borges and Frankignoulle (2002) and Borges et al. (2006). On an annual basis, the ECH and the SBNS act as a mean sink of respectively -0.08 and -0.15 mol C m^{-2} yr^{-1} over 1994–2004 period.

However, the simulated air–sea CO_2 fluxes show marked spatial variations (Fig. 8) that follow the surface pCO_2 patterns (Fig. 5). In winter, offshore waters are a sink for atmospheric CO_2 (range -1.2 to -6.2 mmol C m^{-2} d^{-1}; Fig. 8a), but acts as a source of CO_2 in

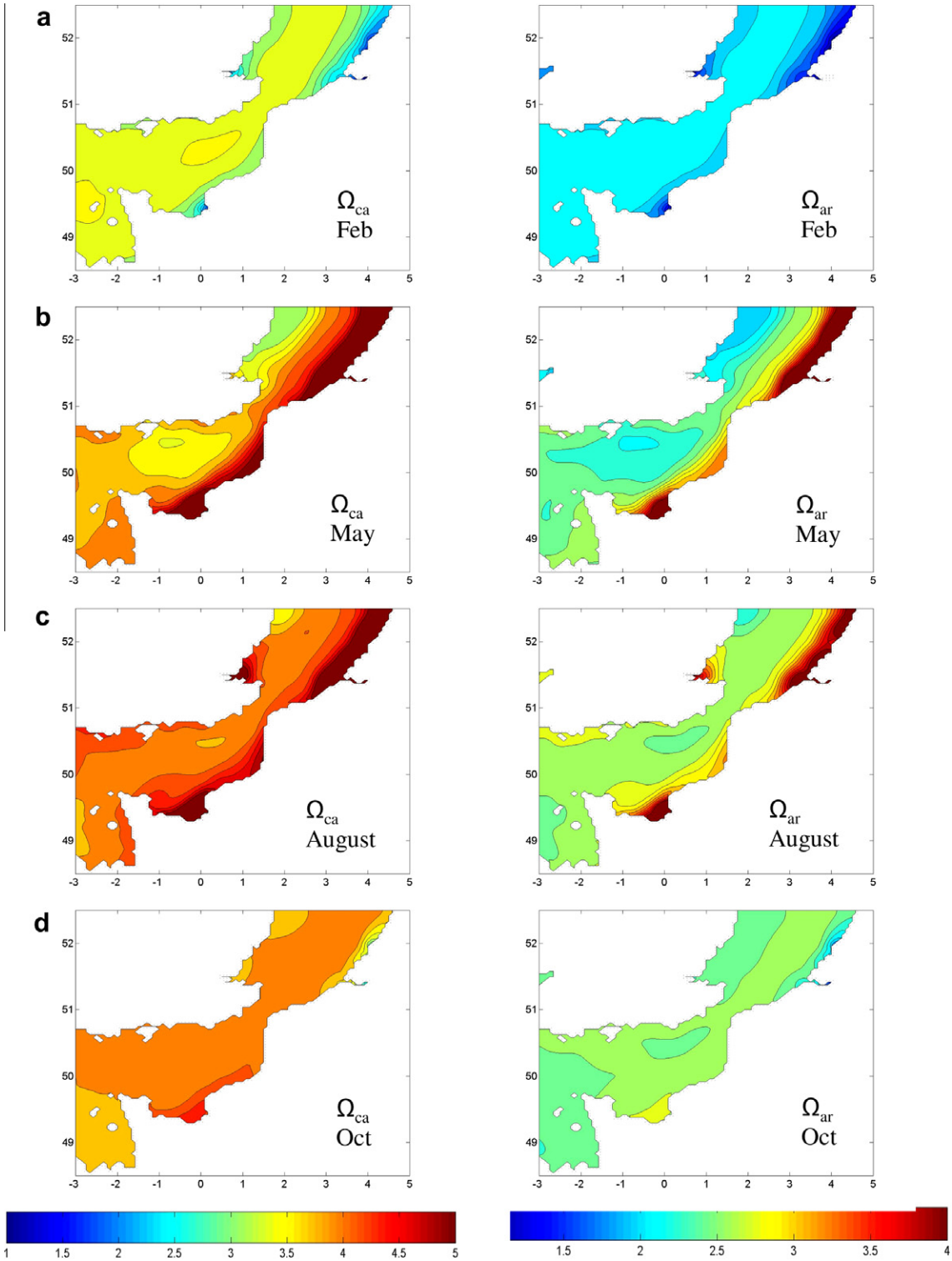

Fig. 6. Spatial distribution of climatological (1994–2004) monthly averaged saturation state of calcite (Ω_{ca}) (left panels) and saturation state of aragonite (Ω_{ar}) (right panels) simulated in February, May, August and October, in the English Channel and Southern Bight of the North Sea.

nearshore waters, especially in the river plumes (range 2.4–12.0 mmol C m^{-2} d^{-1}; Fig. 8a). In spring, the whole domain is a sink of atmospheric CO_2 (range −1.2 to −20.2 mmol C m^{-2} d^{-1}; Fig. 8b) and substantially more intense in nearshore waters (river plumes). One exception is the Thames plume that acts as a source for atmospheric CO_2 with a maximal emission of 4.5 mmol C m^{-2} d^{-1} (Fig. 8b). The situation reverts in summer, when most offshore waters become a source of CO_2 to the atmosphere (range 3.1–13.2 mmol C m^{-2} d^{-1}; Fig. 8c) while a CO_2 sink persists nearshore close to the river plumes (range −2.4 to −11.2 mmol C m^{-2} d^{-1}; Fig. 8c). The CO_2 source is maintained in autumn in offshore waters although less intense than in summer (Fig. 8c and d). Coastal waters

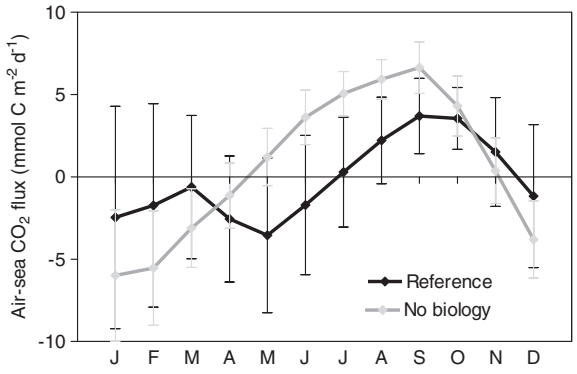

Fig. 7. Seasonal evolution of climatological (1994–2004) monthly averaged air–sea CO_2 fluxes (mmol C m^{-2} d^{-1}) simulated for the reference simulation (black) and for the simulation without biological activities (grey), in the whole domain (English Channel and Southern Bight of the North Sea). Negative fluxes represent a sink of CO_2 from the atmosphere to the ocean, and positive fluxes represent a source of CO_2 from the ocean to the atmosphere.

are close to atmospheric CO_2 equilibrium in autumn while river plumes in the ECH and SBNS act as significant sources of CO_2 to the atmosphere (Fig. 8d).

To appraise the spatio-temporal variability, EOFs were computed on the monthly results estimated for the climatological 1994–2004 period. First and second EOF spatial and temporal modes of the seasonal variability are shown on Fig. 9. Air–sea CO_2 fluxes display a predominant seasonal signal in the first mode that explains 64% of the total variance with the highest positive value of air–sea CO_2 flux (sources) in winter and negative values (sink) in spring and summer (Fig. 9a). The corresponding spatial mode displays a nearshore/offshore gradient, with a marked anomaly near the river mouths and a low anomaly in the open water, due to highest amplitude of seasonal variability in the nearshore waters. The second mode (explaining 24% of the total variance) displays a second seasonal signal with a coherent behaviour at the basin scale except near the north-west UK coastal waters (Fig. 9b). The lowest value of air–sea CO_2 fluxes (sink) are simulated in spring and the highest value (source) in summer and autumn. Then the whole simulated domain acts as a sink for CO_2 in spring and a source in autumn, first and second EOF reflect an opposite seasonality of the air–sea CO_2 flux simulated in offshore and nearshore waters in winter and summer with nearshore waters acting as a sink for CO_2 in summer and a source in winter while the opposite CO_2 flux is simulated in offshore water.

3.3. Biotic and abiotic controls of air–sea CO_2 exchanges

The respective role of the main factors driving the simulated seasonal and spatial variability of air–sea CO_2 fluxes (thermodynamic effect related to SST change *vs.* biological activities) are estimated from the comparison between air–sea CO_2 fluxes obtained with the reference simulation and those simulated when biological processes are cancelled. In the latter scenario, the effect of biological processes are not taken into account in the seawater carbonate dynamics and the simulated variability of air–sea CO_2 fluxes results from the thermodynamic effect of SST changes and, in nearshore waters, from river inputs of DIC. Without biological activity and considering monthly mean climatological air–sea CO_2 fluxes for the 1994–2004 period for the whole model domain, the area acts as a stronger CO_2 sink in winter, a source of CO_2 in spring (instead of a sink of CO_2) and a stronger source of CO_2 in summer compared to the reference simulation (Fig. 7). This comparison

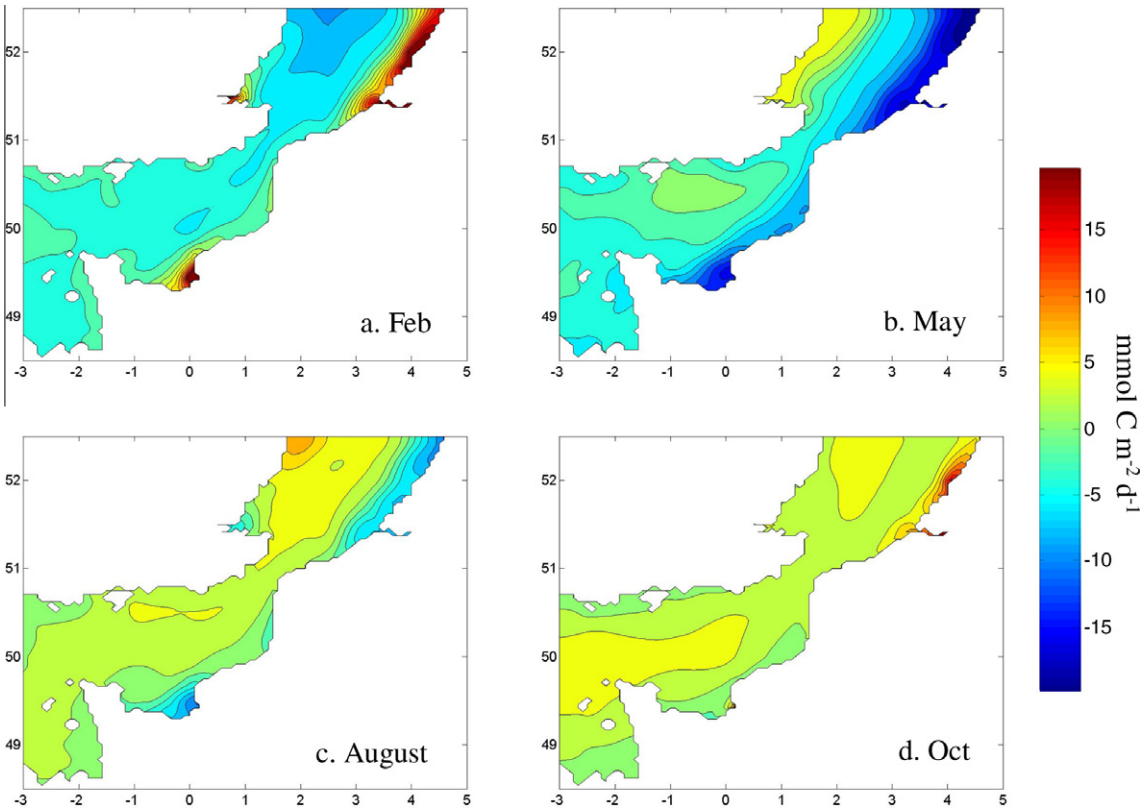

Fig. 8. Spatial distribution of climatological (1994–2004) monthly averaged daily air–sea CO_2 fluxes (mmol C m^{-2} d^{-1}) simulated in February (a), May (b), August (c) and October (d), for the reference simulation in the English Channel and Southern Bight of the North Sea. Negative fluxes represent a sink of CO_2 from the atmosphere to the ocean, and positive fluxes represent a source of CO_2 from the ocean to the atmosphere.

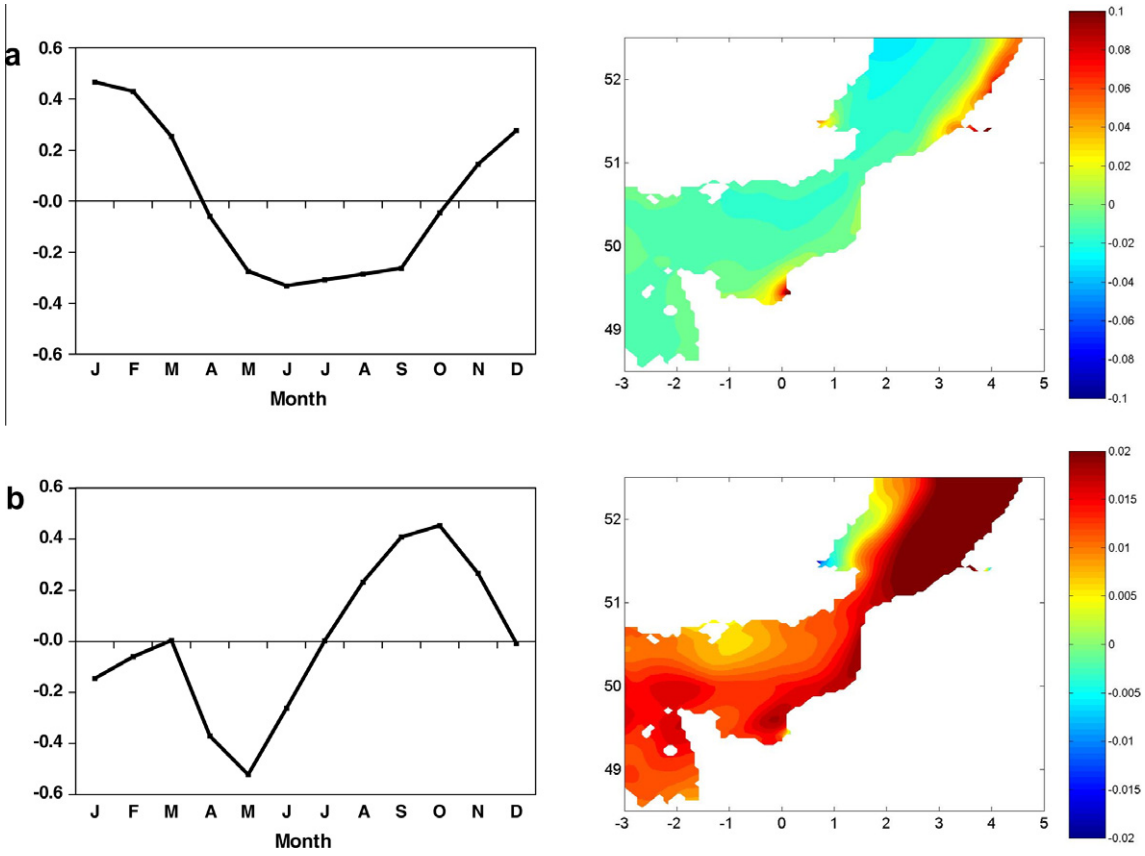

Fig. 9. First (a) and second (b) EOF modes of the spatial and temporal variability of air–sea CO_2 fluxes in the English Channel and Southern Bight of the North Sea, for the 1994–2004 reference simulation.

shows the major importance of biological processes in spring when they revert the sign of the air–sea CO_2 flux simulated in the whole area.

The relative importance of thermodynamic and biological forcings on the spatial gradients and seasonality of air–sea CO_2 fluxes is investigated for the year 2004 (reference simulation). Fig. 10 compares air–sea CO_2 fluxes obtained with the reference simulation (Fig. 10a–d) and those simulated when biological processes are cancelled (Fig. 10e–h). The difference between the two simulations (Fig. 10i–l) allows to appraise the role of biological processes in driving air–sea CO_2 fluxes. SST is the main driver of the sink of atmospheric CO_2 simulated in winter (Fig. 10a, e, and i) in the whole domain while biological (heterotrophic) activity is decreasing the importance of the CO_2 sink. This is particularly marked in the nearshore waters of the eastern SBNS and the Thames mouth, where the simulated source of CO_2 in winter (Fig. 10a, e, and i) is clearly related to heterotrophic activity sustained by the river discharge of organic matter. In spring (Fig. 10b, f, and j), the CO_2 sink simulated in more than 90% of the domain can be attributed to primary production. The low CO_2 sink simulated in the central ECH results from insufficient primary production to counterbalance the increase of surface pCO_2 due to SST increase. In the highly turbid and low-light Thames river plume, primary production is light-limited and the air–sea CO_2 fluxes are driven by the dominance of heterotrophic processes and by river inputs of DIC. In summer (Fig. 10c, g, and k), the increase of SST alone would lead to a strong source of CO_2 to the atmosphere in the whole domain but the magnitude of the source is buffered by autotrophic activity and the sign of the flux is reverted in nearshore waters where biological activity is responsible for the simulated CO_2 sink. Considering the discrepancies between observations and simulations in summer (August, Fig. 3a), the influence of autotrophic processes in the model could be overestimated at this period of the year in the nearshore waters, leading to the simulation of CO_2 under-saturation and a CO_2 sink. In autumn (Fig. 10d, h, and l), offshore primary production is insufficient to balance the thermodynamic effect of the SST increase that results in a source of CO_2 to the atmosphere. In contrast, the CO_2 source simulated in nearshore waters of the eastern SBNS is related to the degradation of organic matter modulated by the temperature effect. On an annual basis, the CO_2 sink simulated in the ECH and the SBNS decreases of 0.6 and of 0.5 mol C m^{-2} yr^{-1} without biology, respectively (Table 1).

3.4. Impact of carbon and nutrient river loads on the annual mean air–sea CO_2 fluxes and seawater carbonate chemistry

The impact of carbon and nutrient river loads on the annual mean air–sea CO_2 fluxes and seawater carbonate chemistry is analyzed considering the simulation for year 2004. On an annual scale, simulations in 2004 show that estuarine plumes act as a source of CO_2 to the atmosphere, and coastal waters act as a sink for atmospheric CO_2 and offshore waters as neutral or moderate sinks of atmospheric CO_2 (Fig. 11a). To analyse the spatial extension of the impact of river loads, two nearshore areas, characterized by a SSS lower than 32 and comprised between 32 and 34, respectively, are defined (Fig. 1).

Spatial integration of annual air–sea CO_2 flux yields a low sink for atmospheric CO_2 (-0.13 mol C m^{-2} yr^{-1}) for the ECH, while the SBNS is close to the equilibrium ($+0.04$ mol C m^{-2} yr^{-1}) in 2004. The nearshore coastal waters of SSS < 32 in the vicinity of the Seine, the Thames and the Scheldt/Rhine river mouths are emitting CO_2 at a rate of 0.31, 1.83 and 0.24 mol C m^{-2} yr^{-1},

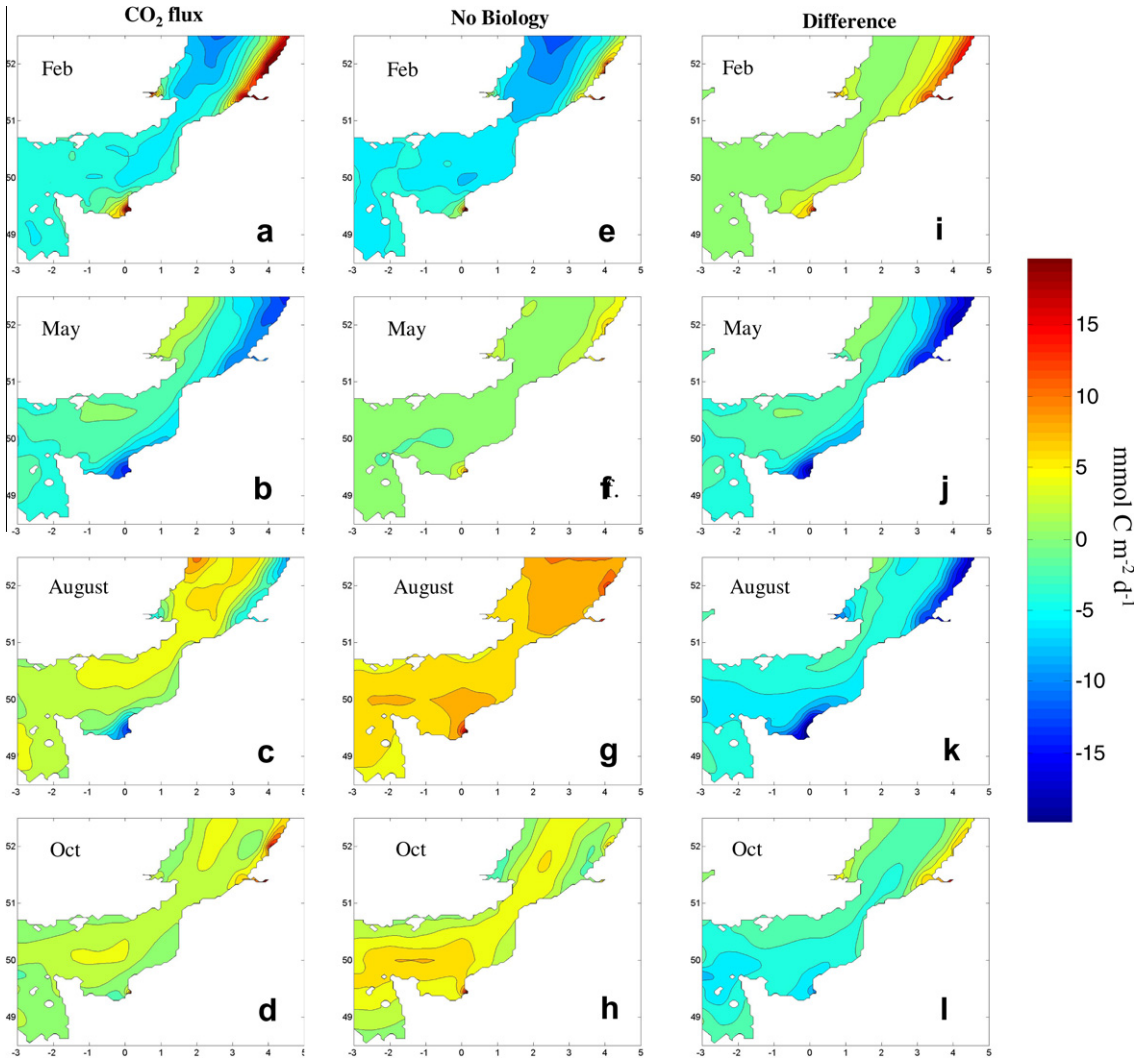

Fig. 10. Spatial distribution of monthly averaged daily air–sea CO_2 fluxes (mmol C m^{-2} d^{-1}) simulated in February, May, August and October 2004, for the reference simulation (left panels), for the simulation without biological activities (central panels) and the difference between both simulations (right panels), in the English Channel and Southern Bight of the North Sea. Negative fluxes represent a sink of CO_2 from the atmosphere to the ocean, and positive fluxes represent a source of CO_2 from the ocean to the atmosphere.

respectively. Coastal water masses of intermediate salinity ($32 < SSS < 34$) act as low CO_2 sources (0.06 mol C m^{-2} yr^{-1} near the Thames river mouth) or as sinks for atmospheric CO_2 (-0.79 and -0.22 mol C m^{-2} yr^{-1} respectively near the Seine and the Scheldt/Rhine river mouths, respectively; Fig. 11a). The different behaviour simulated near the Thames river mouth compared to other estuarine plumes of the domain results from a higher SPM concentration (Mills et al., 1994) and consequently stronger light limitation of primary production (Lacroix et al., submitted for publication).

The corresponding annual mean of pH is about 8.08 over the whole domain (ranging spatially between 7.89 and 8.18; Fig. 11b). The annual mean of Ω_{ca} in 2004 is 3.83 and 3.72 in the ECH and the SBNS, respectively (ranging spatially between 2.63 and 4.67; Fig. 11c), and the annual mean of Ω_{ar} is 2.46 and 2.41 in the ECH and the SBNS, respectively (ranging spatially between 1.63 and 2.96; Fig. 11d). The general spatial pattern of pH, Ω_{ca} and Ω_{ar} is characterized by higher values nearshore than offshore in particular in the plume of the Seine and the combined plume of the Scheldt and Rhine.

In order to estimate the impact of carbon and nutrient river loads on the annual air–sea CO_2 fluxes and seawater carbonate chemistry, sensitivity scenarios were carried out by: (i) cancelling the organic carbon inputs from the rivers, (ii) considering DIC loads in equilibrium with the atmosphere (using for the freshwater end-member DIC computed from TA and atmospheric pCO_2), (iii) cancelling nutrient inputs from the rivers and (iv) cancelling both the organic carbon and nutrient inputs from the rivers. These scenarios were applied for the year 2004 on all rivers at the same time and the resulting annual air–sea CO_2 fluxes and seawater carbonate chemistry were compared to the reference simulation as well as to that obtained by cancelling the biological activity as described in Section 3.3. (Table 1). The area affected by the river loads in terms of air–sea CO_2 fluxes is estimated by computing the difference between the reference simulation and each of the four scenarios cancelling river loads (Fig. 12).

When biological activity is set to zero, the ECH and the SBNS act as a source of CO_2 at the same rate of $\sim$0.5 mol C m^{-2} yr^{-1} (Table 1). Inorganic and organic carbon loads from all rivers drive a source of CO_2 to the atmosphere, and nutrient loads drive a sink for atmospheric CO_2, and the change in air–sea CO_2 fluxes is stronger in the nearshore waters (Table 1; Fig. 12). The impact on air–sea CO_2 fluxes of organic and inorganic carbon loads is mainly confined to the water masses of $SSS < 34$ (Table 1; Fig. 12a and b), while the

Table 1
Sensitivity analysis of the effect of river carbon and nutrient loads on the annually integrated air–sea CO_2 flux (mol C m^{-2} yr^{-1}), pH, saturation state of calcite (Ω_{ca}) and of aragonite (Ω_{ar}) for the English Channel (ECH), the Southern Bight of the North Sea (SBNS) and areas of salinity <32 or between 32 and 34 for year 2004.

			SSS < 32			32 < SSS < 34		
	ECH	SBNS	Seine	Thames	Scheldt/Rhine	Seine	Thames	Scheldt/Rhine
CO_2 flux (mol C m^{-2} yr^{-1})								
Reference	−0.13	0.04	0.31	1.83	0.24	−0.79	0.06	−0.22
Without Biology	0.47	0.5	2.87	1.7	1.58	0.88	0.37	0.67
Organic C loads = 0	−0.18	−0.18	−0.64	0.56	−0.59	−1.18	−0.32	−0.52
DIC at atmospheric equilibrium	−0.18	−0.19	−1.61	0.35	−0.74	−1.19	−0.17	−0.43
Nutrient loads = 0	0.16	0.82	4.67	3.88	3.15	1.25	1.15	1.05
Nutrient and C loads = 0	0.00	0.08	−0.75	0.08	−0.44	−0.07	0.27	0.26
pH								
Reference	8.084	8.078	8.159	8.073	8.127	8.142	8.092	8.109
Without Biology	8.057	8.05	8.020	8.037	8.034	8.054	8.059	8.055
Organic C loads = 0	8.086	8.085	8.195	8.121	8.154	8.158	8.108	8.119
DIC at atmospheric equilibrium	8.086	8.085	8.231	8.124	8.158	8.158	8.101	8.116
Nutrient loads = 0	8.072	8.046	7.977	7.967	8.012	8.048	8.032	8.054
Nutrient and C loads = 0	8.075	8.057	8.081	8.041	8.064	8.073	8.049	8.063
Ω_{ca}								
Reference	3.852	3.777	4.499	3.728	3.926	4.311	3.832	3.974
Without Biology	3.648	3.566	3.411	3.448	3.315	3.620	3.584	3.569
Organic C loads = 0	3.868	3.832	4.815	4.088	4.138	4.443	3.95	4.053
DIC at atmospheric equilibrium	3.869	3.831	5.162	4.118	4.167	4.443	3.9	4.029
Nutrient loads = 0	3.759	3.551	3.135	3.003	3.123	3.585	3.401	3.562
Nutrient and C loads = 0	3.753	3.511	3.156	2.968	2.988	3.555	3.346	3.485
Ω_{ar}								
Reference	2.462	2.407	2.846	2.359	2.477	2.747	2.44	2.532
Without Biology	2.331	2.273	2.157	2.182	2.092	2.307	2.282	2.274
Organic C loads = 0	2.472	2.441	3.045	2.587	2.611	2.831	2.515	2.582
DIC at atmospheric equilibrium	2.472	2.441	3.263	2.605	2.629	2.831	2.483	2.567
Nutrient loads = 0	2.402	2.263	1.983	1.901	1.971	2.285	2.166	2.270
Nutrient and C loads = 0	2.399	2.238	1.996	1.878	1.886	2.266	2.131	2.220

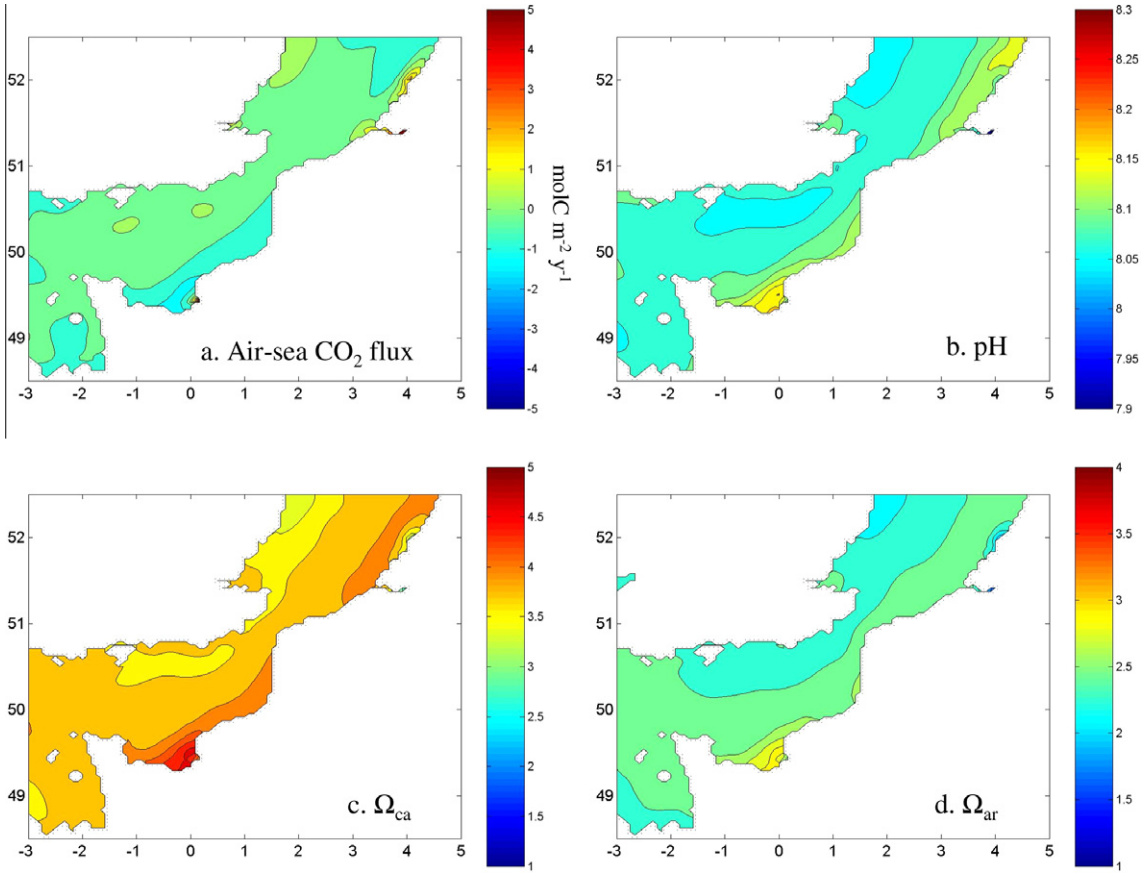

Fig. 11. Spatial distribution of annual means of: (a) air–sea CO_2 flux (mol C m^{-2} yr^{-1}), (b) pH, (c) saturation state of calcite (Ω_{ca}) and (d) saturation state of aragonite (Ω_{ar}) simulated for 2004, in the English Channel and Southern Bight of the North Sea.

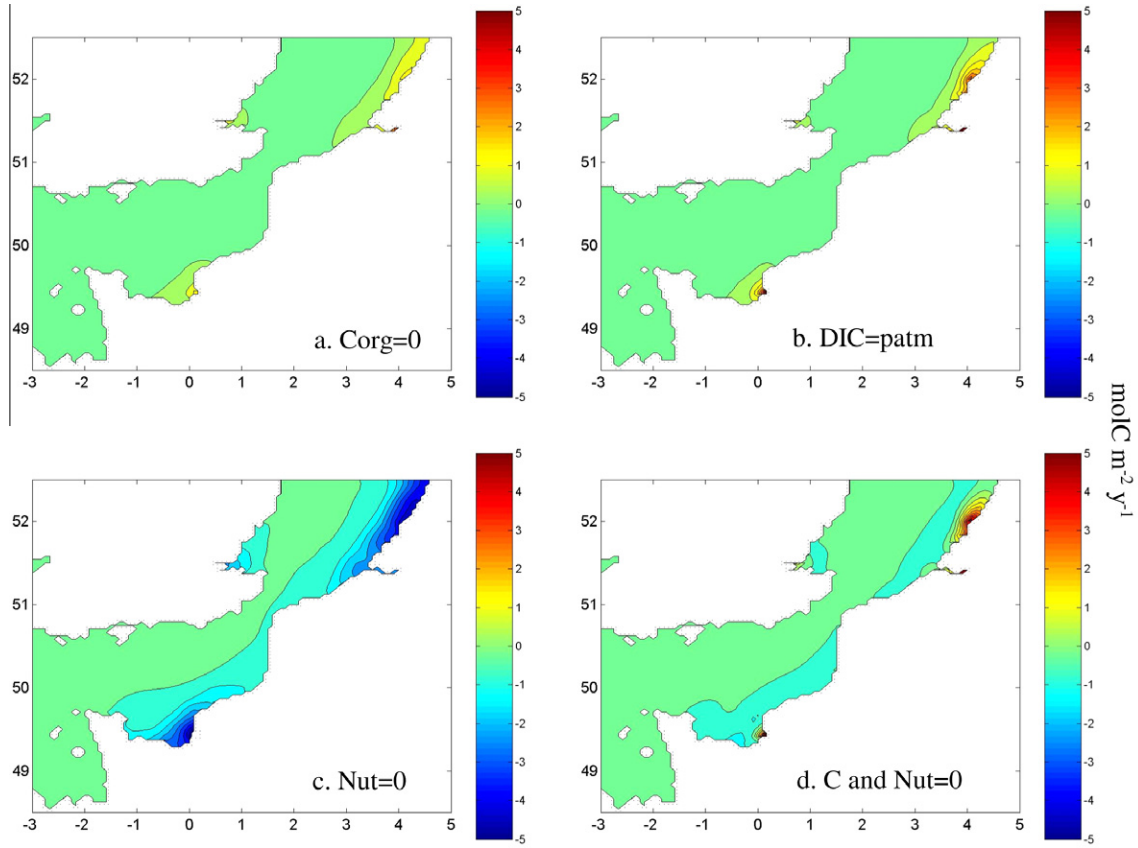

Fig. 12. The anomaly of the air–sea CO_2 flux (mol C m^{-2} yr^{-1}) computed as the difference between the reference simulation and the scenarios for: (a) organic carbon loads at zero, (b), DIC loads in equilibrium with the atmosphere, (c) nutrient loads at zero and (d) carbon and nutrient loads at zero, in the English Channel and the Southern Bight of the North Sea.

impact of nutrient loads from the rivers also propagates in offshore waters along the French, Belgian and Dutch coasts (Fig. 12c). This suggests that river nutrients are impacting offshore waters as they are not completely consumed nearshore. In contrast, continental organic matter brought by rivers are locally degraded and emitted CO_2 to the atmosphere, as well as river DIC inputs, hence they have an impact confined to nearshore waters. In the absence of river organic or inorganic carbon loads, the annual CO_2 sink computed in the ECH increases by 0.05 mol C m^{-2} yr^{-1} (38% of the CO_2 sink given by the reference simulation) while the SBNS shifts from neutral (0.04 mol C m^{-2} yr^{-1}) to a CO_2 sink (−0.19 mol C m^{-2} yr^{-1}). The nearshore waters (SSS < 32) shift from a CO_2 source to a CO_2 sink, except in the vicinity of the Thames river mouth where heterotrophic processes still dominate photosynthesis due to light limitation. At the scale of the whole domain, the impact of organic *vs.* inorganic carbon river loads on the annual air–sea CO_2 flux is similar, but the CO_2 source driven by the supply of inorganic carbon is greater than the one associated to organic loads in the vicinity of the rivers (SSS < 32). In the absence of nutrient river loads, an annual source of CO_2 is simulated for the whole domain (Table 1) and river nutrient loads have a greater impact on air–sea CO_2 fluxes than organic and inorganic carbon river loads (Table 1; Fig. 12).

Annually, the combined effect of carbon and nutrient river loads is to increase the sink of CO_2 in the ECH and the SBNS but to a lower extent than river nutrients loads alone. However, the impact of river loads varies spatially, carbon and nutrient loads lead to a CO_2 source in nearshore coastal waters (SSS < 32) and to a sink for CO_2 in the rest of the domain (Table 1, Fig. 12d).

The same scenarios were applied to quantify the impact of biological activity sustained by river loads on annual means of pH, Ω_{ca} and Ω_{ar} (Table 1). In the ECH and SBNS, biological activity sustains higher pH and Ω_{ca} and Ω_{ar} values. This is related to nutrient river loads, while organic and inorganic carbon loads tend to decrease pH and Ω_{ca} and Ω_{ar} values (Table 1). As observed for air–sea CO_2 flux, the impact of nutrient river loads on pH and Ω_{ca} and Ω_{ar} is higher than the organic and inorganic carbon river loads, and mainly confined in the nearshore waters.

3.5. Inter-annual variability of air–sea CO_2 fluxes and seawater carbonate chemistry

Fig. 13 shows the evolution of annual air–sea CO_2 flux (in mol C m^{-2} yr^{-1}; Fig. 13a), SST (Fig. 13b), SSS (Fig. 13c) and Net Ecosystem Production (NEP in mol C m^{-2} yr^{-1}; Fig. 13d) simulated from 1994 to 2004 in the ECH and the SBNS. The annual air–sea CO_2 fluxes in the ECH tend to increase from −0.21 to 0.13 mol C m^{-2} yr^{-1} between 1994 and 2001 after what a CO_2 sink of about −0.11 mol C m^{-2} yr^{-1} is again simulated between 2002 and 2004 (Fig. 13a). In the SBNS, the annual air–sea CO_2 fluxes vary from −0.33 to 0.22 mol C m^{-2} yr^{-1}, with a decrease of the atmospheric CO_2 sink from 1994 to 2004. The increase of air–sea CO_2 fluxes simulated in the ECH in 2000 and 2001 seems to propagate in the SBNS. These annual air–sea CO_2 flux values are in good agreement with available data in the area (Kempe and Pegler, 1991; Hoppema, 1991; Bakker et al., 1996; Frankignoulle and Borges, 2001; Borges and Frankignoulle, 1999, 2002, 2003; Thomas et al., 2004; Schiettecatte et al., 2006, 2007; Borges et al., 2008a; Omar et al., 2010).

From 1994 to 2004, annual SST and SSS show important variability without any characteristic trend (Fig. 13b and c). In addition, annual NEP (Fig. 13d) simulated in the ECH varies between

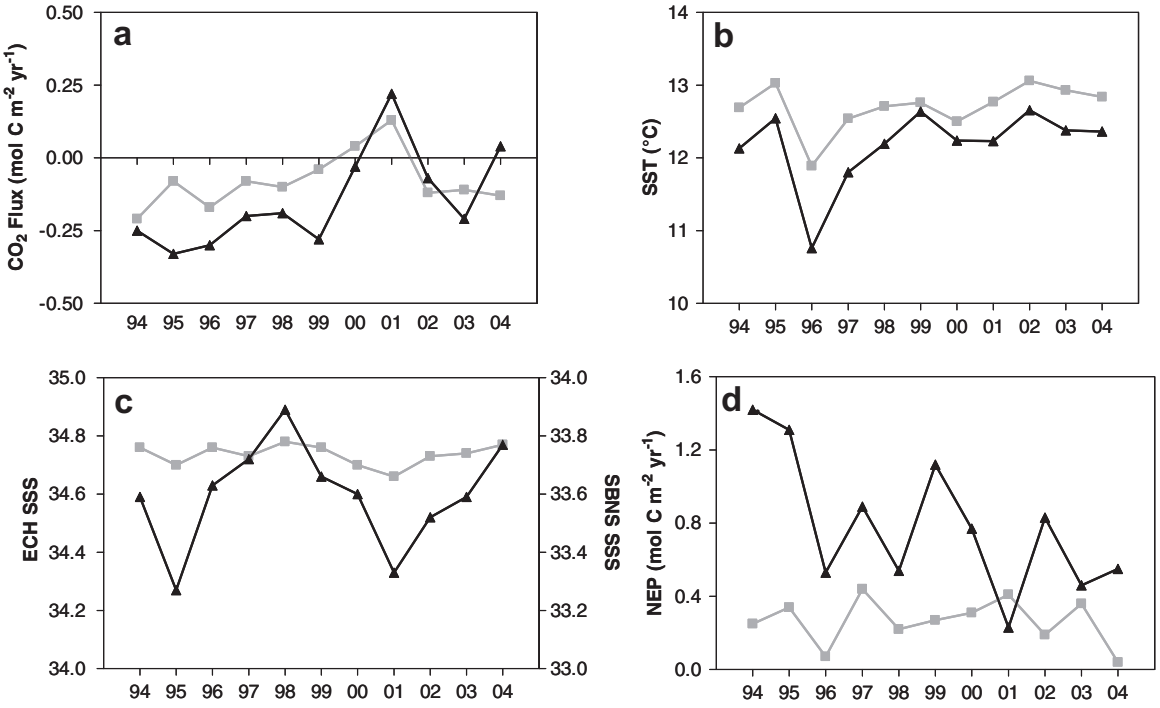

Fig. 13. Annual: (a) air–sea CO_2 flux (in mol C m^{-2} yr^{-1}), (b) SST (°C), (c) SSS and (d) NEP (mol C m^{-2} yr^{-1}) simulated from 1994 to 2004 in the English Channel (ECH) (grey) and the Southern Bight of the North Sea (SBNS) (black).

0.45 and 0.04 mol C m^{-2} yr^{-1} with no general trend. In the SBNS on the contrary, NEP tends to decrease from 1.4 to 0.5 mol C m^{-2} yr^{-1} between 1994 and 2004. Correlations between annual variations of air–sea CO_2 fluxes and SST, SSS and NEP were computed using a cumulative sum (Cusum) function (e.g., Beamish et al., 1999). On an annual basis, no significant relationship was found between air–sea CO_2 fluxes and SST in either of the two areas. No relationship was found between annual air–sea CO_2 flux and SSS in the SBNS, but, in the ECH, the increase of the contribution of Atlantic waters (i.e., increase of SSS) enhances the sink for atmospheric CO_2 (r^2 = 0.78). In the SNBS, the inter-annual variability of annual air–sea CO_2 fluxes is partly explained by NEP (r^2 = 0.61), the annual CO_2 sink increasing when the annual NEP increases. This shows that the drivers of inter-annual variations of air–sea CO_2 fluxes in coastal environments are complex (multiple drivers), not readily predicted by a single forcing, and can be different even into adjacent and connected environments such as the ECH and the SBNS.

The first three modes of the EOF analysis of the inter-annual variability of air–sea CO_2 fluxes (computed based on annual results) are presented on Fig. 14. Air–sea CO_2 fluxes display a predominant inter-annual signal in the first mode that explains 49% of the total variance (Fig. 14a). The corresponding spatial mode displays a synoptic behaviour of the whole domain with an amplitude of the variance most pronounced in estuaries and in the vicinity of rivers and reflects the variability of river discharge. The highest positive air–sea CO_2 fluxes (sources) were simulated in 1994, 1995, 2000, 2001 and 2002 and the lowest air–sea CO_2 fluxes (sink) in 1996, 1997 and 2004. The second mode (explaining 19% of the total variance) displays a second inter-annual signal (Fig. 14b) with an opposed anomaly near the river mouth and along the coast lines, especially along the French coast. The highest anomaly is observed at the boundaries of the domain with the lowest and the highest values in 1994 and 2001, respectively. The third mode, explaining 13% of the total variance shows an opposite behaviour in the northeast coastal waters of the SBNS, especially near the Scheldt mouth and the associated river plume and coastal waters, than in the rest of the domain. The air–sea CO_2 flux largely varies between 1994 and 2004, and the anomaly is highest in 2004 and shows opposite anomaly in the Belgian and Netherlands coastal waters than in the rest of the domain.

Changes in SST, wind strength and direction, atmospheric pCO_2 and carbon and nutrient river loads directly and/or indirectly affect decadal variations of the exchange of CO_2 across the air–sea interface. Wind speed directly acts on the gas transfer velocity affecting the intensity of the air–sea CO_2 flux but also on the wind-driven currents in the ECH and the SBNS and the extent of the river plumes. Wind can either contain fresh waters close to the coast or advect them offshore. The direction of air–sea CO_2 flux depends on the air–sea gradient of pCO_2 that is a function of atmospheric CO_2 and seawater pCO_2. Seawater pCO_2 will depend of SST (solubility coefficient) and of biological activity, itself function of carbon and inorganic nutrient inputs. The contribution of each of these forcings on the simulated annual air–sea CO_2 flux is investigated based on the comparison between annual air–sea CO_2 fluxes computed using the 1994–2004 reference forcings and annual air–sea CO_2 fluxes computed using constant forcings: (i) a constant value of atmospheric pCO_2 of 360 ppm (Fig. 15a), (ii) 1994 wind speed and direction (Fig. 15b), (iii) 1994 SST (Fig. 15c) and (iv) 1994 river loads (Fig. 15d). Evolution of the atmospheric pCO_2 and river loads are shown Fig. 2 and wind speed and direction are reported by Lacroix et al. (2004).

The comparison between the reference annual air–sea CO_2 fluxes and those obtained by imposing a constant value of atmospheric pCO_2 of 360 ppm (Fig. 15a) suggests that the increase of atmospheric CO_2 from 1994 to 2004 results in a CO_2 uptake by about 0.02–0.06 mol C m^{-2} yr^{-1}. The impact of the atmospheric CO_2 increase is similar in the ECH and the SBNS with no effect on the inter-annual fluctuations. Wind strength and direction have a strong impact on the annual air–sea CO_2 flux in the SBNS and in particular in the ECH where this forcing can modify the direction of the annual simulated flux (Fig. 15b). Wind speed acts directly on the gas transfer velocity and the intensity of the air–sea CO_2

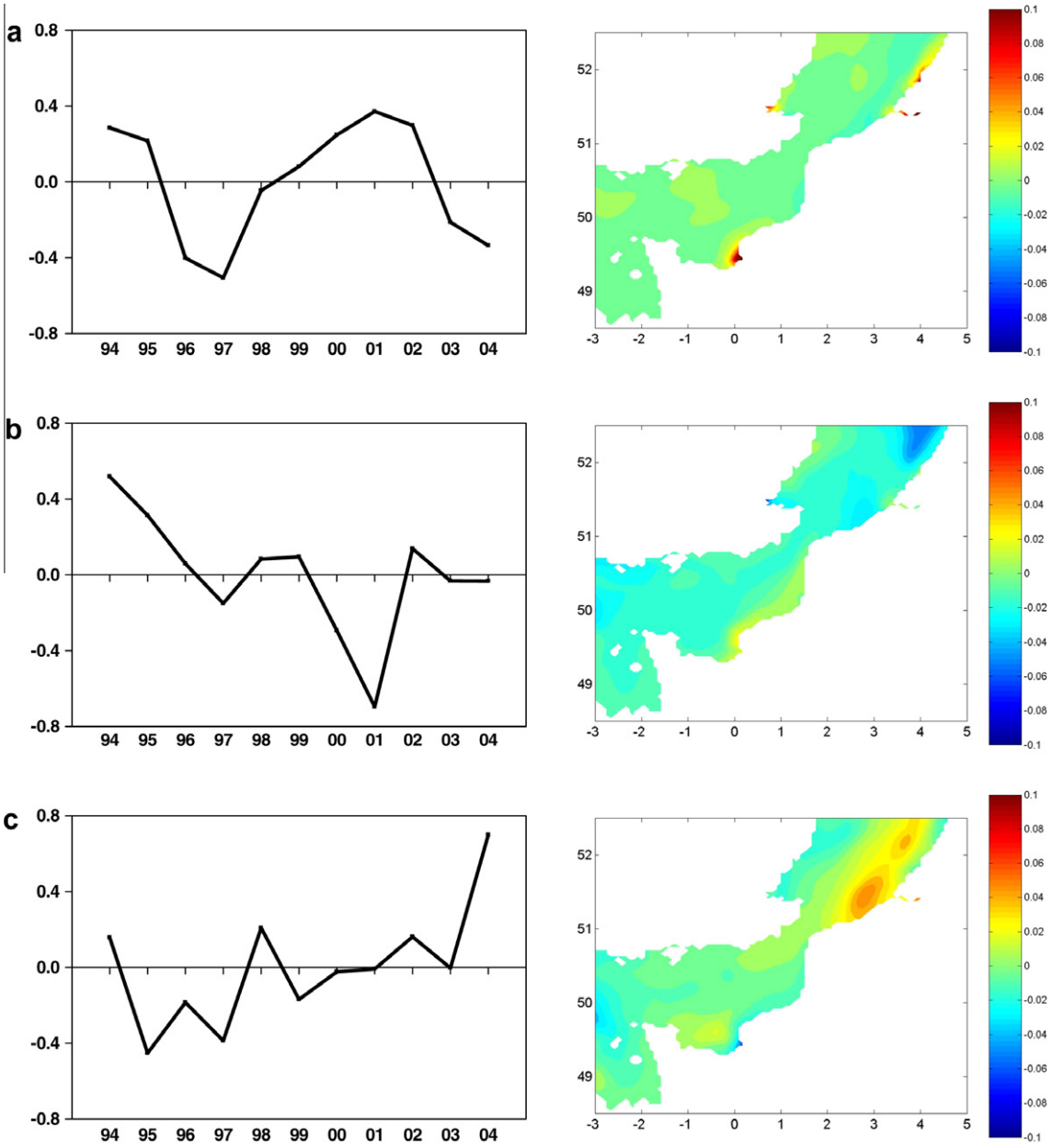

Fig. 14. Three modes of EOF spatial and temporal variance of the inter-annual variations of air–sea CO_2 fluxes from 1994 to 2004 in the English Channel and Southern Bight of the North Sea.

flux, and wind speed and direction also act on the relative importance of influx of Atlantic waters and on the extension of the river plumes. The SST variation over the period affects more the air–sea CO_2 flux in the ECH than in the SBNS. An increase of annual SST decreases the annual CO_2 sink and conversely a decrease of annual SST increases the annual CO_2 sink (Fig. 15c). The impact of SST is particularly marked in 1996, a very cold year, leading to a stronger CO_2 sink (Fig. 15c). Carbon and nutrient river loads have little impact on the annual air–sea CO_2 flux simulated in the ECH excepted in 1996 characterized by a very low river inputs. Variations of carbon and nutrient river loads can increase or decrease annual CO_2 flux simulated in the SBNS up to 0.22 and 0.80 mol C m^{-2} yr^{-1}, respectively (Fig. 15d). When using the 1994 river loads for the 1994–2004 period, simulated inter-annual variability is still important but the decreasing trend of the CO_2 sink simulated in the reference simulation is not represented. From 1994 to 2004, nutrient loads (mainly P) have decreased inducing a decrease of the NEP and the CO_2 sink in the area. In conclusion, most of the simulated 1994–2004 variability of air–sea CO_2 fluxes differs from one region to another and is explained by fluctuations in wind strength and direction in the ECH and in river loads in the SBNS (Fig. 15). Similarly, Previdi et al. (2009) show that the main drivers of inter-annual variability of the air–sea CO_2 flux in the northeast US continental shelf differ spatially. In the Middle Atlantic Bight where inter-annual variations of air–sea CO_2 fluxes are mainly related to changes in near-surface wind speed, and in the Gulf of Maine, variability of surface water pCO_2 is controlled by changes in SST and NEP.

The importance of river loads in driving inter-annual variability in the SBNS was also highlighted by the EOF analysis of inter-annual variations: the first mode reflects the changes on river discharge (Fig. 14a), while the second mode (Fig. 14b) reflects the increasing limitation of primary production by P availability due to changes in P river loads with respect to N river inputs (Fig. 2).

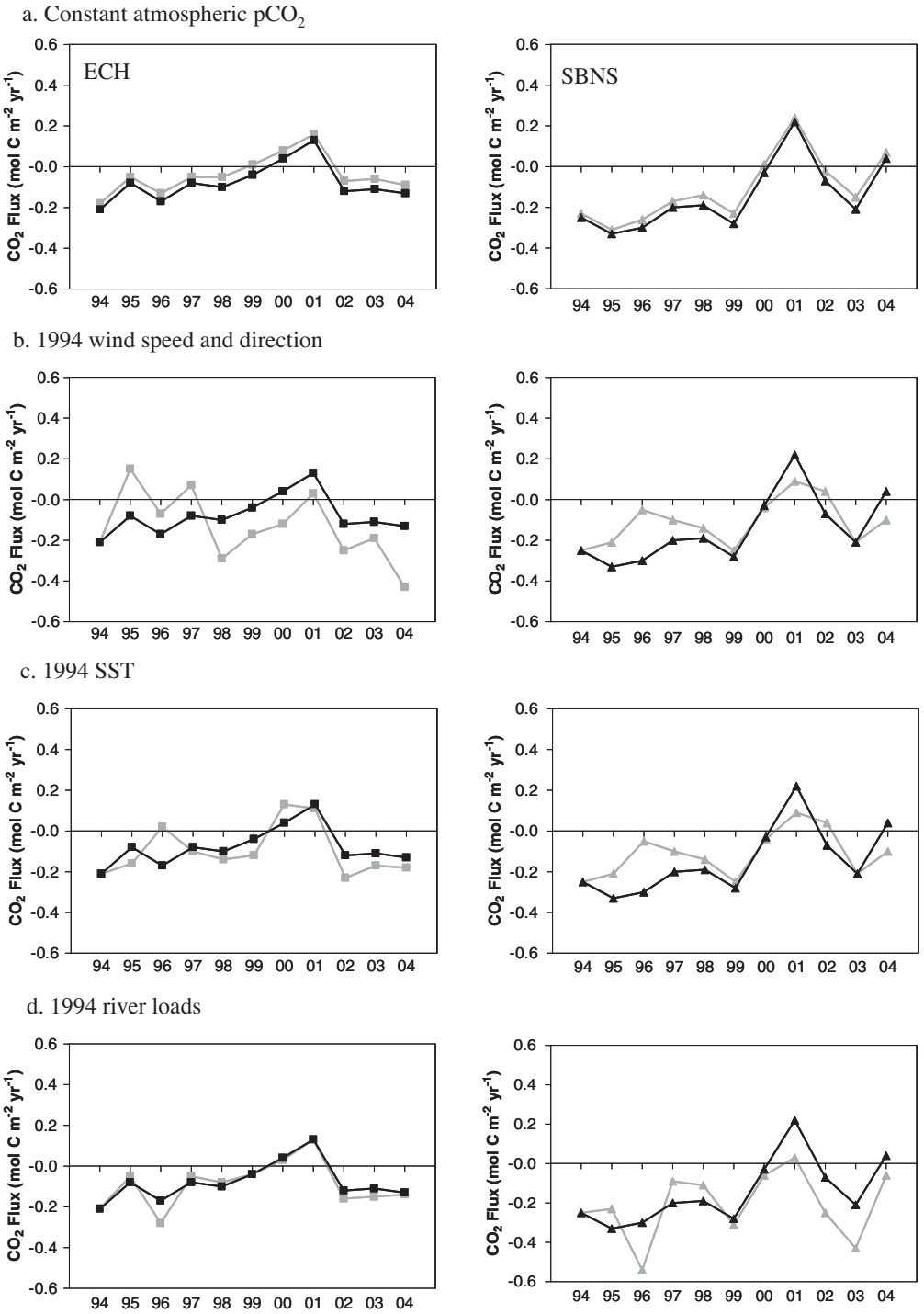

Fig. 15. Annual air–sea CO_2 flux (in mol C m^{-2} yr^{-1}) simulated from 1994 to 2004 in the English Channel (ECH) (left) and the Southern Bight of the North Sea (SBNS) (right) using the 1994–2004 forcing for atmospheric pCO_2, wind speed and direction, sea water temperature and river loads compared to annual air–sea CO_2 flux computed using: (a) a constant atmospheric pCO_2 of 360 ppm, (b) 1994 wind speed and direction, (c) 1994 SST and (d) 1994 river loads. The black line corresponds to the reference simulation and the grey line to the considered scenario.

In the ECH and the SBNS, a significant decrease in pH was simulated for the 1994–2004 period (Table 2). The pH changes are larger in the SBNS than in the ECH. In the ECH, the annual pH decrease is close to the one expected if surface water had tracked the increase of atmospheric CO_2 during the same period (Table 2). The Ω_{ca} and Ω_{ar} decreasing trends are only statistically significant when excluding the colder 1996 year within the considered time period. Yet, the decrease of Ω_{ca} and Ω_{ar} in the ECH is close to that expected considering only atmospheric CO_2 increase. In the SBNS, the observed trends in pH, Ω_{ca} and Ω_{ar} (excluding year 1996) are stronger than those expected from ocean acidification. This can be attributed to the decrease of primary production and NEP in the SBNS due to the increase of N:P river loads, that has led to a gradual limitation and decline of primary production since the mid-1980s (Lancelot et al., 2007; Gypens et al., 2009; Borges and Gypens, 2010). Hence, changes in nutrient delivery from rivers

Table 2
Rate of change per year ± standard error (r^2; p) of pH, saturation state of calcite (Ω_{ca}) and of aragonite (Ω_{ar}) from 1994 to 2004 in the English Channel (ECH) and the Southern Bight of the North Sea (SBNS). The rate of change due to atmospheric pCO_2 alone was computed using the 1994 conditions except for pCO_2 in seawater that increases at the rate of atmospheric pCO_2 based on the data from Mace Head. The rate of change due to SST change alone was computed using the 1994 conditions except for SST. For the rate of change of Ω_{ca} and Ω_{ar}, year 1996 was excluded from the analysis since it was an anomalously cold year.

	ECH	SBNS
Reference run		
pH	−0.00183 ± 0.00026 (r^2 = 0.85; p < 0,0001)	−0.0032 ± 0.00038 (r^2 = 0.88; p < 0.0001)
Ω_{ca}	−0.0053 ± 0.0046 (r^2 = 0.13; p = 0.28)	−0.0122 ± 0.0082 (r^2 = 0.2, p = 0.17)
Ω_{ar}	−0.0032 ± 0.0031 (r^2 = 0.11; p = 0.32)	−0.0074 ± 0.0054 (r^2 = 0.17, p = 0.201)
Reference run without 1996 year		
pH	−0.00182 ± 0.00028 (r^2 = 0.84; p = 0,0002)	−0.0032 ± 0.00043 (r^2 = 0.88; p < 0.0001)
Ω_{ca}	−0.0084 ± 0.0035 (r^2 = 0.42; p = 0.04)	−0.018 ± 0.0062 (r^2 = 0.52, p = 0.019)
Ω_{ar}	−0.0053 ± 0.0023 (r^2 = 0.39; p = 0.05)	−0.0112 ± 0.0039 (r^2 = 0.5, p = 0.02)
Due to atmospheric pCO_2 increase alone		
pH	−0.00196 ± 0.00004 (r^2 = 0.99; p < 0.0001)	−0.00196 ± 0.00004 (r^2 = 0.99; p < 0.0001)
Ω_{ca}	−0.0137 ± 0.0003 (r^2 = 0.99; p < 0.0001)	−0.0143 ± 0.0003 (r^2 = 0.99; p < 0.0001)
Ω_{ar}	−0.0087 ± 0.0002 (r^2 = 0.99; p < 0.0001)	−.0091 ± 0.0002 (r^2 = 0.99; p < 0.0001)
Due to SST change alone		
pH	0.000004635 ± 0.000006031 (r^2 = 0.06875; p = 0.4643)	0.000006649 ± 0.000007841 (r^2 = 0.08246; p = 0.4211)
Ω_{ca}	0.001913 ± 0.002445 (r^2 = 0.07106; p = 0.4566)	0.002696 ± 0.003327 (r^2 = 0.07588; p = 0.4411)
Ω_{ar}	0.001292 ± 0.001651 (r^2 = 0.07109; p = 0.4565)	0.001816 ± 0.002242 (r^2 = 0.07578; p = 0.4414)

due to management policies on the regulation of nutrient inputs from rivers to the coastal zone can over time lead in nearshore environments such as the SBNS to stronger changes in carbonate chemistry than ocean acidification due to changes in primary production and NEP (Borges and Gypens, 2010). During the same period, SST increased in both the ECH and the SBNS at a rate of ~0.02 ± 0.02 °C yr^{-1} (Fig. 15c). The change that would have resulted from SST increase alone for pH, Ω_{ca} and Ω_{ar} is several orders of magnitude lower than that given by the reference simulation (Table 2).

4. Conclusions

Continental shelf systems play an important role in the exchange of CO_2 between the atmosphere and ocean, but the magnitude of this flux and the relative contributions of different underlying mechanisms are poorly quantified due to large spatial and temporal environmental gradients and the sparse field measurements of air–sea CO_2 fluxes (Borges, 2005; Borges et al., 2005; Cai et al., 2006; Chen and Borges, 2009; Laruelle et al., 2010). Moreover, in a given shelf system strong inter-annual variability in air–sea CO_2 fluxes can occur due to changes in atmospheric forcing related to large-scale climate oscillations (Friederich et al., 2002; Borges et al., 2008b). Year-to-year changes in meteorological forcing can have profound impacts on ocean temperature, chemistry, vertical mixing and circulation, all of which impact the ocean carbon cycle (McKinley et al., 2004). Quantifying inter-annual variability and the mechanisms that control this variability are therefore a critical component of the estimation of CO_2 fluxes on continental shelves and to understand the current and future role of continental shelves in the oceanic carbon sink. This can be achieved using biogeochemical models such as the one presented in this paper.

Our study shows the high seasonal and inter-annual variability of the distribution of pCO_2 and air–sea CO_2 flux in the ECH and the SBNS and its multiple controlling biotic and abiotic factors. The simulated surface pCO_2 over the 1994–2004 period ranges seasonally from 100 to 750 ppm. As a general pattern, the area acts as a source for CO_2 in autumn and summer and as a sink in winter and spring and the seasonal variation of surface pCO_2 and air–sea CO_2 flux in nearshore waters is mainly controlled by biological activities. During spring and early summer, phytoplankton blooms occur first in nearshore waters and then propagate throughout the whole area inducing important CO_2 under-saturation of surface waters in the whole domain of simulation. In late summer and autumn, the degradation of phytoplankton and the subsequent release of CO_2 induce over-saturation, mainly in the river plumes. Due to the important river loads, spatial variability is superimposed to this seasonal variability, river loads enhancing the importance of biological activities in the river plume and nearshore waters. Freshwater inputs of nutrient and organic matter have an opposite impact on the coastal carbonate chemistry by, respectively, stimulating primary production and heterotrophy; the impact on air–sea CO_2 fluxes of organic and inorganic carbon loads is mainly confined to the water masses of SSS < 34, while the impact of nutrient loads from the rivers also propagates in offshore waters. On an annual basis, the coastal-offshore continuum is then characterized by a succession of CO_2 source in estuarine plumes, CO_2 sink in nearshore coastal waters and neutral or low CO_2 sink in offshore waters. River loads also modify seasonal evolution by stimulating biological activities in nearshore coastal waters and in the area: during winter, river plumes and nearshore waters are oversaturated in CO_2 with respect to the atmosphere (due to heterotrophic activity) while the rest of the domain acts as a sink for CO_2. In offshore waters, the temperature effect on the carbonate system dynamics is higher than biological activity in winter and autumn, but in spring and summer net autotrophy counteracts the effect of temperature increase and reduces the CO_2 source in the whole domain.

On an annual scale, for the 1994–2004 period, the simulated CO_2 fluxes vary between −0.21 and 0.13 mol C m^{-2} yr^{-1}in the ECH and between −0.33 and 0.22 mol C m^{-2} yr^{-1} in the SBNS. Sensitivity scenarios made in this study show that the main processes (meteorological *vs.* hydrodynamic *vs.* anthropogenic) responsible of the year-to-year changes in the CO_2 air–sea flux differ between regions (ECH *vs.* SBN). In the ECH (less influenced by river loads), the inter-annual variations of air–sea CO_2 fluxes are mainly due to changes in SST and in near-surface wind strength and direction, while the inter-annual variability of air–sea CO_2 fluxes simulated in the SBNS is controlled primarily by river loads and changes of primary production (net autotrophy in spring and early summer, and net heterotrophy in winter and autumn). In the SBNS, the decreasing CO_2 sink simulated between 1994 and 2004 can be mainly related to changes in nutrient river loads. From 1994 to 2004, nutrient loads (mainly P) decreased inducing a decrease of the NEP and the CO_2 sink in the area. In the absence of biological activity or without nutrient river loads, the ECH and the SBNS would act as sources for atmospheric CO_2. Variability of wind strength and direction that influences the extent of the river plumes was also identified as an important driver of the magnitude of the annual air–sea CO_2 flux simulated in the area. This highlights the importance of inter-annual variability of air–sea CO_2 fluxes in coastal environments that has been seldom investigated due to sparseness of available field data, but can be accomplished with a well calibrated 3-D regional model.

Acknowledgements

The present work is a contribution to the AMORE (Advanced MOdeling and Research on Eutrophication) project funded by Belgian Science Policy (Contract Nos. EV-11-19 and SD/NS/03A), to the FP6 European Integrated Project CARBOOCEAN (contract no. 511176 (GOCE)), to FP7 European Coordination and support action COCOS (212196), to the TIMOTHY project (P6/13) funded by the Interuniversity Attraction Poles Programme – Belgian State – Belgian Science Policy, to SOLAS and to COST 735. The present work benefited from data obtained in the frame of EU BIOGEST (ENV4-CT96-0213) and Belgian Science Policy CANOPY (CArbon, NitrOgen and Phosphorus cYcling in the North Sea, EV/12/20C) projects. A.V.B. is a F.R.S.-F.N.R.S. research associate, N.G. is a F.R.S.-F.N.R.S. postdoctoral researcher. We acknowledge Alexander Barth and Aida Alvera Azcarate for help in implementing the EOF Matlab scripts, Francisco Werner (Editor) and two anonymous reviewers for constructive comments on a previous version of the manuscript.

References

Algesten, G., Wikner, J., Sobek, S., Tranvik, L.J., Jansson, M., 2004. Seasonal variation of CO_2 saturation in the Gulf of Bothnia: indications of marine net heterotrophy. Global Biogeochemical Cycles 18, GB4021. doi:10.1029/2004GB002232.

Bakker, D.C.E., de Barr, H.J.M., de Wilde, H.P.J., 1996. Dissolved carbon dioxide in Dutch coastal waters. Marine Chemistry 55, 247–263.

Beamish, R.J., Noakes, D.J., McFarlane, G.A., Klyashtorin, L., Ivanov, V.V., Kurashov, V., 1999. The regime concept and natural trends in the production of Pacific salmon. Canadian Journal of Fisheries and Aquatic Sciences 56, 516–526.

Billen, G., Garnier, J., Ficht, A., Cun, C., 2001. Modeling the response of water quality in the Seine river estuary to human activity in its watershed over the last 50 years. Estuaries 24, 977–993.

Billen, G., Garnier, J., Rousseau, V., 2005. Nutrient fluxes and water quality in the drainage network of the Scheldt basin over the last 50 years. Hydrobiologia 540, 47–67.

Borges, A.V., 2005. Do we have enough pieces of the jigsaw to integrate CO_2 fluxes in the Coastal Ocean? Estuaries 28 (1), 3–27.

Borges, A., Frankignoulle, M., 1999. Daily and seasonal variations of the partial pressure of CO_2 in surface seawater along Belgian and southern Dutch coastal areas. Journal of Marine Systems 19 (4), 251–266.

Borges, A.V., Frankignoulle, M., 2002. Distribution and air–water exchange of carbon dioxide in the Scheldt plume off the Belgian coast. Biogeochemistry 59, 41–47.

Borges, A.V., Frankignoulle, M., 2003. Distribution of surface carbon dioxide and air–sea exchange in the English Channel and adjacent areas. Journal of Geophysical Research 108 (5C). doi:10.1029/2000JC000571.

Borges, A.V., Gypens, N., 2010. Carbonate chemistry in the coastal zone responds more strongly to eutrophication than to ocean acidification. Limnology and Oceanography 55, 346–353.

Borges, A.V., Delille, B., Frankignoulle, M., 2005. Budgeting sinks and sources of CO_2 in the coastal ocean: diversity of ecosystems counts. Geophysical Research Letters 32, L14601. doi:10.1029/2005GL023053.

Borges, A.V., Schiettecatte, L.-S., Abril, G., Delille, B., Gazeau, F., 2006. Carbon dioxide in European coastal waters. Estuarine, Coastal and Shelf Science 70 (3), 375–387.

Borges, A.V., Ruddick, K., Schiettecatte, L.-S., Delille, B., 2008a. Net ecosystem production and carbon dioxide fluxes in the Scheldt estuarine plume. BMC Ecology 8, 15. doi:10.1186/1472-6785-8-15.

Borges, A.V., Tilbrook, B., Metzl, N., Lenton, A., Delille, B., 2008b. Inter-annual variability of the carbon dioxide oceanic sink south of Tasmania. Biogeosciences 5, 141–155.

Cai, W.-J., Wang, Y., 1998. The chemistry, fluxes, and sources of carbon dioxide in the estuarine waters of the Satilla and Altamaha Rivers, Georgia. Limnology and Oceanography 43 (4), 657–668.

Cai, W.-J., Wang, Z.A., Wang, Y., 2003. The role of marsh-dominated heterotrophic continental margins in transport of CO_2 between the atmosphere, the land–sea interface and the ocean. Geophysical Research Letters 30, 1849. doi:10.1029/2003GL017633.

Cai, W.-J., Dai, M.H., Wang, Y.C., 2006. Air–sea exchange of carbon dioxide in ocean margins: a province-based synthesis. Geophysical Research Letters 33, L12603. doi:10.1029/2006GL026219.

Cai, W.-J., Guo, X., Chen, C.T.A., Dai, M., Zhang, L., Zhai, W., Lohrenz, S.E., Yin, K., Harrison, P.J., Wang, Y., 2008. A comparative overview of weathering intensity and HCO_3^- flux in the world's major rivers with emphasis on the Changjiang, Huanghe, Zhujiang (Pearl) and Mississippi Rivers. Continental Shelf Research 28 (1–2), 1538–1549.

Chen, C.T.A., Borges, A.V., 2009. Reconciling opposing views on carbon cycling in the coastal ocean: continental shelves as sinks and nearshore ecosystems as sources of atmospheric CO_2. Deep-Sea Research II 56 (8–10), 578–590.

Chierici, M., Fransson, A., 2009. Calcium carbonate saturation in the surface water of the Arctic Ocean: undersaturation in freshwater influenced shelves. Biogeosciences 6, 2421–2432.

Dickson, A.G., 1990. Thermodynamics of the dissociation of boric acid in synthetic sea water from 273.15 to 298.15 K. Deep-Sea Research Part A 37, 755–766.

Doney, S.C., Mahowald, N., Lima, I., Feely, R.A., Mackenzie, F.T., Lamarque, J.-F., Rasch, P.J., 2007. Impact of anthropogenic atmospheric nitrogen and sulfur deposition on ocean acidification and the inorganic carbon system. Proceedings of the National Academy of Sciences 104 (37), 14580–14585.

Doney, S.C., Fabry, V.J., Feely, R.A., Kleypas, J.A., 2009. ocean acidification: the other CO_2 problem. Annual Review of Marine Science 1, 169–192.

Fabry, V.J., Seibel, B.A., Feely, R.A., Orr, J.C., 2008. Impacts of ocean acidification on marine fauna and ecosystem processes. Journal of Marine Science 65, 414–432.

Feely, R.A., Sabine, C.L., Hernandez-Ayon, J.M., Ianson, D., Hales, B., 2008. Evidence for upwelling of corrosive "acidified" water onto the continental shelf. Science 320, 1490–1492.

Frankignoulle, M., Borges, A.V., 2001. European continental shelf as a significant sink for atmospheric carbon dioxide. Global Biogeochemical Cycles 15 (3), 569–576.

Frankignoulle, M., Bourge, I., Wollast, R., 1996. Atmospheric CO_2 fluxes in a highly polluted estuary (The Scheldt). Limnology and Oceanography 41 (2), 365–369.

Frankignoulle, M., Abril, G., Borges, A.V., Bourge, I., Canon, C., Delille, B., Libert, E., Théate, J.-M., 1998. Carbon dioxide emission from European estuaries. Science 282, 434–436.

Friederich, G.E., Walz, P.M., Burczynski, M.G., Chavez, F.P., 2002. Inorganic carbon in the central California upwelling system during the 1997–1999 El Niño-La Niña events. Progress in Oceanography 54 (1–4), 185–203.

Gledhill, D.K., Wanninkhof, R., Millero, F.J., Eakin, M., 2008. Ocean acidification of the greater Caribbean region 1996–2006. Journal of Geophysical Research 113, C10031. doi:10.1029/2007JC004629.

Gypens, N., Lancelot, C., Borges, A.V., 2004. Carbon dynamics and CO_2 air–sea exchanges in the eutrophied coastal waters of the Southern Bight of the North Sea: a modelling study. Biogeosciences 1, 147–157.

Gypens, N., Borges, A.V., Lancelot, C., 2009. Effect of eutrophication on air–sea CO_2 fluxes in the coastal Southern North Sea: a model study of the past 50 years. Global Change Biology 15 (4), 1040–1056.

Hoppema, J.M.J., 1991. The seasonal behaviour of carbon dioxide and oxygen in the coastal North Sea along the Netherlands. Netherlands Journal of Sea Research 28, 167–179.

Jiang, L.-Q., Cai, W.-J., Wanninkhof, R., Wang, Y., Hüger, H., 2008. Air–sea CO_2 fluxes on the US South Atlantic Bight: spatial and seasonal variability. Journal of Geophysical Research 113, C07019. doi:10.1029/2007JC004366.

Kempe, S., Pegler, K., 1991. Sinks and sources of CO_2 in coastal seas: the North Sea. Tellus 43B, 224–235.

Kleypas, J.A., Feely, R.A., Fabry, V.J., Langdon, C., Sabine, C.L., Robbins, L.L., 2006. In: Impacts of Ocean Acidification on Coral Reefs and Other Marine Calcifiers: A Guide for Future Research, Report of a Workshop Held 18–20 April 2005, St. Petersburg, FL, sponsored by NSF, NOAA, and the US Geological Survey, 88 pp.

Körtzinger, A., 2003. A significant CO_2 sink in the tropical Atlantic Ocean associated with the Amazon River plume. Geophysical Research Letters 30 (24), 2287. doi:10.1029/2003GL018841.

Lacroix, G., Ruddick, K., Ozer, J., Lancelot, C., 2004. Modelling the impact of the Scheldt and Rhine/Meuse plumes on the salinity distribution in Belgian waters (Southern North Sea). Journal of Sea Research 52, 149–163.

Lacroix, G., Ruddick, K., Gypens, N., Lancelot, C., 2007a. Modelling the relative impact of rivers (Scheldt/Rhine/Seine) and Western Channel waters on the nutrient and diatoms/Phaeocystis distributions in Belgian waters (Southern North Sea). Continental Shelf Research 27 (10-11), 1422–1446.

Lacroix, G., Ruddick, K., Park, Y., Gypens, N., Lancelot, C., 2007b. Validation of the 3D biogeochemical model MIRO&CO with field nutrient and phytoplankton data and MERIS-derived surface chlorophyll a images. Journal of Marine Systems 64 (1–4), 66–88.

Lacroix, G., Sirjacobs, D., Ruddick, K., Park, Y., Beckers, J.-M. and Lancelot, C., submitted for publication. Spatial variability of the spring bloom timing in the Southern North Sea investigated by MIRO&CO-3D and remote sensing. Journal of Marine Systems.

Lancelot, C., Spitz, Y., Gypens, N., Ruddick, K., Becquevort, S., Rousseau, V., Lacroix, G., Billen, G., 2005. Modelling diatom and Phaeocystis blooms and nutrient cycles in the Southern Bight of the North Sea: the MIRO model. Marine Ecology Progress Series 289, 63–78.

Lancelot, C., Gypens, N., Billen, G., Garnier, J., Roubeix, V., 2007. Testing an integrated river–ocean mathematical tool for linking marine eutrophication to land use: the *Phaeocystis*-dominated Belgian coastal zone (Southern North Sea) over the past 50 years. Journal of Marine System 64, 216–228.

Laruelle, G.G., Dürr, H.H., Slomp, C.P., Borges, A.V., 2010. Evaluation of sinks and sources of CO_2 in the global coastal ocean using a spatially-explicit typology of estuaries and continental shelves. Geophysical Research Letters 37, L15607. doi:10.1029/2010GL043691.

Liu, K.K., Iseki, K., Chao, S.-Y., 2000. Continental margin carbon fluxes. In: Hansson, R.B., Ducklow, H.W., Field, J.G. (Eds.), The Changing Ocean Carbon Cycle: A midterm synthesis of the Joint Global Ocean Flux Study. Cambridge University Press, Cambridge, pp. 187–239.

Loewe, P., 2003. Weekly North Sea SST Analyses since 1968. In: Hydrographie, O.d.a.h.b.B.f.S.u. (Ed.), D-20305 Hamburg, P.O. Box 301220, Germany.

McKinley, G.A., Follows, M.J., Marshall, J., 2004. Mechanisms of air–sea CO_2 flux variability in the equatorial Pacific and the North Atlantic. Global Biogeochemical Cycles 18, GB2011. doi:10.1029/2003GB002179.

Mehrbach, C., Culberson, C.H., Hawley, J.E., Pytkowicz, R.M., 1973. Measurements of the apparent dissociation constants of carbonic acid in seawater at atmospheric pressure. Limnology and Oceanography 18, 897–907.

Mills, D.K., Tett, P.B., Novarino, G., 1994. The spring bloom in the South Western North Sea in 1989. Netherlands Journal of Sea Research 33 (1), 65–80.
Mucci, A., 1983. The solubility of calcite and aragonite in seawater at various salinities, temperatures, and one atmosphere total pressure. American Journal of Science 283, 781–799.
Nightingale, P.D., Malin, G., Law, C.S., Watson, A.J., Liss, P.S., Liddicoat, M.I., Boutin, J., Upstill-Goddard, R.C., 2000. In situ evaluation of air–sea gas exchange parameterizations using novel conservative and volatile tracers. Global Biogeochemical Cycles 14, 373–387.
Omar, A.M., Olsen, A., Johannessen, T., Hoppema, M., Thomas, H., Borges, A.V., 2010. Spatiotemporal variations of fCO_2 in the North Sea. Ocean Science 6, 77–89.
Omstedt, A., Gustafsson, E., Wesslander, K., 2009. Modelling the uptake and release of carbon dioxide in the Baltic Sea surface water. Continental Shelf Research 29, 870–885.
Previdi, M., Fennel, K., Wilkin, J., Haidvogel, D., 2009. Interannual variability in atmospheric CO_2 uptake on the northeast US continental shelf. Journal of Geophysical Research 114, G04003. doi:10.1029/2008JG000881.
Salisbury, J., Green, M., Hunt, C., Campbell, J., 2008. Coastal acidification by rivers: a new threat to shellfish? Eos Transactions AGU 89 (50), 513.
Salisbury, J., Vandemark, D., Hunt, C., Campbell, J., Jonsson, B., Mahadevan, A., McGillis, W., Xue, H., 2009. Episodic riverine influence on surface DIC in the coastal Gulf of Maine. Estuarine, Coastal and Shelf Science 82, 108–118.
Schiettecatte, L.-S., Gazeau, F., Van der Zee, C., Brion, N., Borges, A.V., 2006. Time series of the partial pressure of carbon dioxide (2001–2004) and preliminary inorganic carbon budget in the Scheldt plume (Belgian coast waters). Geochemistry, Geophysics, Geosystems (G3) 7, Q06009. doi:10.1029/2005GC001161.
Schiettecatte, L.-S., Thomas, H., Bozec, Y., Borges, A.V., 2007. High temporal coverage of carbon dioxide measurements in the Southern Bight of the North Sea. Marine Chemistry 106 (1–2), 161–173.
Takahashi, T., Sutherland, S.C., Wanninkhof, R., Sweeney, C., Feely, R.A., Chipman, D.W., Hales, B., Friederich, G., Chavez, F., Sabine, C., Watson, A., Bakker, D.C.E., Schuster, U., Metzl, N., Yoshikawa-Inoue, Hi., Ishii, M., Midorikawa, T., Nojiri, Y., Körtzinger, A., Steinhoff, T., Hoppema, M., Olafsson, J., Arnarson, T.S., Tilbrook, B., Johannessen, T., Olsen, A., Bellerby, R., Wong, C.S., Delille, B., Bates, N.R., de Baar, H.J.W., 2009. Climatological mean and decadal change in surface ocean pCO_2, and net sea-air CO_2 flux over the global oceans. Deep-Sea Research II 56 (8–10), 554–577.
Thomas, H., Bozec, Y., Elkalay, K., De Baar, H.J.W., 2004. Enhanced open ocean storage of CO_2 from shelf sea pumping. Science 304 (5673), 1005–1008.
Tsunogai, S., Watanabe, S., Sato, T., 1999. Is there a "continental shelf pump" for the absorption of atmospheric CO_2? Tellus Series A 51, 701–712.
Weiss, R.F., 1974. Carbon dioxide in water and seawater: the solubility of a non-ideal gas. Marine Chemistry 2, 203–215.
Wesslander, K., Omstedt, A., Schneider, B., 2010. Inter-annual and seasonal variations in the air–sea CO_2 balance in the central Baltic Sea and the Kattegat. Continental Shelf Research 30, 1511–1521.
Wikle, C.K., 2002. Spatio-temporal methods in climatology. In: El-Shaarawi, A.H., Jureckova, J. (Eds.), Encyclopedia of Life Support Systems (EOLSS). Eolss, Oxford, UK. Developed Under the Auspices of the UNESCO, <http://www.eolss.net>.